NTNU

Norwegian University of
Science and Technology

Impact of Variable-Speed Hydro on Power System Frequency Stability

Espen Aronsveen

Master of Energy and Environmental Engineering
Submission date: June 2018
Supervisor: Kjetil Uhlen, IEL

Norwegian University of Science and Technology
Department of Electric Power Engineering

Abstract

There is a growing concern that the decreasing share of rotating masses in the power system, caused by the increasing generation of solar and wind power, will lead to frequency problems. Photovoltaic panels and wind turbines are connected to the grid via power electronic interfaces, and are therefore non-synchronous sources that do not contribute to frequency control. The kinetic energy in the rotating masses is the power system's first defense against disturbances and large faults. If the synchronous generation sources, such as hydropower, are replaced by non-synchronous generation, and a large fault occurs, the power system could experience severe frequency problems. Variable-speed hydro is proposed as a possible solution to this problem.

Primary frequency control in Norway and Sweden is today exclusively performed by hydropower plants utilizing droop control. By connecting a hydropower plant to the grid via a frequency converter, the plant can run on variable speed and release more kinetic energy during frequency drops. In this thesis the impact of variable-speed hydro on the system frequency is studied, by developing a simplified power system model in Simulink® based on the swing equation and DC power flow. The model is verified against a higher-order AC model in a test network, before optimal control of the variable-speed plant is investigated.

The control variable for the variable-speed plant is the frequency deviation from the nominal frequency, meaning a large drop in frequency leads to a large contribution during the fault. Only the size of the fault was found to be of importance to the variable-speed plant's contribution to frequency containment, not the location. The location of the variable-speed plant itself did not have significant impact on the results either, only the share of variable-speed capacity. The improved ability to contain the frequency nadir was relatively much larger with small shares introduced. The improvement had a decreasing trend with greater shares of variable-speed capacity in the system. Variable-speed hydro technology shows great promise in the field of primary frequency control, and could play an important role in securing the frequency stability in the future power system.

Sammendrag

En problemstilling for fremtidens kraftsystem er at den avtagende andelen av roterende masser i kraftsystemet, forårsaket av den økende produksjonen fra sol- og vindkraft, vil føre til frekvensproblemer. Solcellepaneler og vindturbiner er koblet til nettet via kraftelektroniske omformere, og er derfor ikke-synkrone produksjonskilder som ikke kan brukes som primærreserver. Den kinetiske energien i de roterende massene er kraftnettets første forsvar mot driftsforstyrrelser. Hvis de synkrone produksjonskildene, som for eksempel vannkraft, erstattes av ikke-synkrone kilder, og en større driftsfortyrrelse forekommer, kan kraftsystemet oppleve alvorlige frekvensproblemer. Vannkraftverk på variabelt turtall har blitt foreslått som en mulig løsning på dette problemet.

Vannkraftverk med statikkinnstilling er i Norge og Sverige i dag den eneste typen kraftproduksjon som blir tatt i bruk som primærreserve. Ved å koble inn en frekvensomformer mellom et vannkraftverk og nettet, kan vannkraftverket kjøre på variabelt turtall og frigjøre mer kinetisk energi under frekvensfallsituasjoner. I denne masteroppgaven studeres virkningen av variabelt turtall på systemfrekvensen ved å utvikle en forenklet modell av kraftsystemet i Simulink® basert på svingelikningen og en DC lastflyt. Modellen sammenlignes med en høyere ordens AC-modell i et testnettverk, før optimal styring av vannkraftverket med variabelt turtall undersøkes.

Kontrollvariabelen for vannkraftverket med variabelt turtall er frekvensavviket fra den nominelle frekvensen, noe som betyr at et stort frekvensfall fører til et høyt bidrag under driftsforstyrrelsen. Kun størrelsen på driftsforstyrrelsen viste seg å av betydning for hvor mye vannkraftverket med variablet turtall bidro til å minke frekvensfallet, ikke lokasjonen. Hvor i nettet vannkraftverket med variabelt turtall var plassert hadde heller ikke betydelig innvirkning på resultatene; bare andelen av den totale produksjonskapasiteten med variabelt turtall. Den forbedrede evnen til å begrense frekvensenfallet var relativt sett mye større med små andeler innført. Forbedringen hadde en avtagende trend når større andeler av den totale produksjonskapasiteten kjørtes på variabelt turtall. Variabelt turtallsteknologi viser stort potensiale som primærreserve, og kan spille en viktig rolle for å sikre frekvensstabiliteten i fremtidens kraftsystem.

Preface

This Master's Thesis concludes my Master of Science (MsC) degree in Energy and Environmental Engineering with the Department of Electric Power Engineering at the Norwegian University of Science and Technology (NTNU). The thesis treats concepts from power system stability, with focus on improving the frequency stability in the Nordic grid. The work was performed under the supervision of Professor Kjetil Uhlen with the Department of Electric Power Engineering NTNU.

The project work conducted during the previous fall laid the foundation for the thesis and potential future work within power system stability in particular, and research in general. I have gained knowledge within several other areas as well, such as power electronics and control theory. I would like to express my sincerest gratitude to my supervisor, Kjetil Uhlen, for sharing his knowledge within these areas of research, and his guidance in general. A special thanks also to my girlfriend, Katrine Merkesdal Hall, for helping me with proofreading.

Trondheim, 06.06.2018

Espen Aronsveen

Contents

List of Figures

List of Tables

Chapter 1

Introduction

1.1 Background

The European power system is experiencing a major energy transition, with the decarbonization goals stated in the Paris agreement as the key driver for the increasing production from renewable energy sources. Generation from wind and photovoltaic (PV) are showing the largest growth rates. The transition is evident in the Nordic power system as well, and Statnett predicts that solar and wind will make up approximately 50 % of the total energy production in the Nordic system in 2040 [2]. Even though this development is positive with respect to decarbonization and a sustainable energy production, this trend could potentially cause the power system to suffer from a stability point of view. There is growing concern that the increased production of renewables are creating inertia problems for the grid. PV and wind power uses power electronic interfaces to connect to the grid, and are therefore not contributing to the system inertia. Neither do the interconnecting HVDC cables. A decreased amount of rotational masses connected to the grid could potentially lead to frequency instability following a disturbance.

Frequency containment reserves (FCR) is the power system's first defence against frequency problems caused by a disturbance. Hydropower is the main resource used to provide FCR services in the Nordic grid, due to its flexibility [3]. However, with more intermittent production from PV and wind, the power system would benefit from an even higher degree of flexibility from its generation sources. Variable-speed hydro (VSH) is a possible solution, with reportedly

several benefits. There are two technical solutions that enable this ability; a doubly-fed induction machine (DFIM) and a converter-fed synchronous machine (CFSM). The DFIM has the stator of the machine directly connected to the grid, while the rotor windings are connected via a frequency converter. A CFSM, on the other hand, is connected to the grid via a full-rated frequency converter. The high power ratings required by the converter makes this a difficult and expensive solution as of today. The power ratings of the converter for the DFIM do not normally exceed 30 % of the plant's rated power [4], which makes for the preferred configuration for high power ratings. However, this technology only provides around 10 % of variable-speed variation to the plant. It is expected that the power ratings of converters will increase, especially because of the development of modular multilevel converters (MMC). CFSM could thus be the VSH technology of the future.

There are several reported benefits of variable-speed hydro. The main benefit is the ability to control power in pump mode [4], which makes it able to store excess energy in a more flexible manner. Other reported benefits are improved voltage control, higher hydraulic efficiency for the power plant and longer lifetime for the turbine. The drawbacks of implementing VSH are the cost and the profitability, which is a challenge due to small price differences between on- and off peak prices. This is probably the reason why VSH in the Nordic system is only a research topic, and why there are no such plants present in the grid, nor under construction. There is one VSH plant already in operation in Switzerland, and the results have been promising [5]. Two more variable-speed plants, Linth-Limmern and Nant-de-Drance, are under construction [6, 7].

The feature of interest for this thesis is VSH's ability to offer instantaneous active power injection, also referred to as the flywheel effect. This ability is unlocked by the fast and dynamic control of the voltage source converter (VSC), and has the potential to make the hydropower plant work more efficiently as FCR. This thesis aims at developing a model that is able to evaluate the performance of VSH in the Nordic grid during frequency drops caused by large disturbances.

1.2 Objectives

The main objective of this thesis is to develop a model that is able to quantify the power system impact of variable-speed hydro, with focus on frequency stability. The goal is to make a flexible and fast model, able to run scenarios for a future Nordic power system. Validation methods should be applied to the model in order to justify assumptions that are made, and ensure the reliability of the results.

1.3 Scope

The scope of this study is frequency analysis. Other aspects of power system stability, such as rotor angle stability and voltage stability, will not be considered. The study is limited to under-frequency events and to how variable-speed hydro could minimize the effects of large disturbances. Even though a major benefit of variable-speed hydro is the ability to control power in pump mode, this operation mode will not be considered. Because of this, only one converter is necessary, and the control strategy of a back-to-back voltage source converter is therefore outside the scope of this thesis.

The power plant under study has a converter-fed synchronous machine. The most popular variable-speed technology today is a doubly-fed induction machine, since it does not require a full-scaled converter. However, with the development within the field of power electronics and the increased power ratings of converters, the converter-fed synchronous machine is expected to become the preferred technology. The operational limits of the machine are not considered. In reality, the rotor's deviation from nominal speed is limited by physical phenomena, such as cavitation and vibrations. The operational limits imposed by these phenomena are ignored for the sake of simplicity.

1.4 Structure of the Report

Chapter 1 - *Introduction*, presents the background for the research topic, and gives a brief overview of the objectives and scope of the work.

Chapter 2, *Theory*, provides an introduction to the main theory required to read the report.

Chapter 3, *Method*, introduces the software used in the thesis and explains the modeling approach for both the DC- and AC model. Assumptions and simplifications made to the models are pointed out and justified.

Chapter 4, *Model*, presents in detail the model elements including the hydropower plant, the electromechanical dynamics, the voltage source converter and the MATLAB® function blocks. The power system networks used for the case studies are presented and illustrated.

Chapter 5, *Simulations and Results*, contains the most important results obtained in this study. The model is validated by comparing it to an AC model, and an optimal control scheme is developed for the variable-speed plant. Scenarios are made in order to study the effects of variable-speed hydro, both in today's grid and in the grid of the future.

Chapter 6, *Summary*, summarizes the conducted work and the main results from Chapter 5, before some concluding remarks are given. Suggestions for future work are also included.

Chapter 2

Theory

2.1 Power System Stability

The term power system stability is defined in [8] as "the ability of an electric power system, for a given initial operating condition, to regain a state of operating equilibrium after being subjected to a physical disturbance, with most system variables bounded so that practically the entire system remains intact." Interconnected power systems are subjected to a variety of disturbances, both small and large. Small disturbances, such as load changes, occur continuously and the system must be able to adjust to the operating conditions. A robust power system should also be able to survive large disturbances, such as a short-circuit on a transmission line or the loss of a large generator. When studying power system stability, one must understand which physical phenomena are relevant and which variables are of importance. Both fast electromagnetic and slow thermodynamic phenomena can affect stability, but the main physical characteristic connected with power system stability is electromechanical phenomena [1]. The main variables of interest in stability analysis are rotor angle, voltage magnitudes and frequency. This thesis will focus on frequency stability.

2.2 Frequency Stability

The reference frequency of the Nordic power system is at 50.00 Hz. The frequency is continuously monitored to ensure stable operation of the power system, where the total generation

should be equal to the total consumption. When this operating condition is met, the power system is in equilibrium and the system frequency is constant. A severe fault or large disturbance can result in a long-term mismatch between generation and load. Frequency stability refers to the system's ability to maintain a steady system frequency following such an event [8]. The goal is to maintain or restore equilibrium between generation and load, with minimal unintentional loss of load. The difference between produced and consumed power is initially covered by the kinetic energy of the rotating masses in the system, such as turbines and synchronous generators. As the machines are slowing down, the frequency will change [1]. The frequency change is commonly divided into four stages, which will be discussed later. First one must study the swing equation to understand the main physics behind the concept of frequency change in a power system.

2.3 The Swing Equation

The swing equation is derived from Newton's second law for rotation. The equation relates the acceleration or deceleration of a synchronous generator and turbine to the imbalance between mechanical- and electrical torque. This section provides a brief explanation and derivation of the swing equation, which is highly relevant for this thesis. A more detailed explanation can be found in [1]. Newton's second law for rotation is given as

$$J\frac{d\omega_m}{dt} + D_d\omega_m = \tau_t - \tau_e \tag{2.1}$$

where J is the total moment of inertia of the turbine and generator rotor in kgm^2, ω_m is the rotor shaft velocity in mechanical rad/s, D_d is the damping torque coefficient in Nms, τ_t is the torque produced by the turbine and τ_e is the counteractive electromagnetic torque. In steady state the rotor angle speed is equal to the synchronous speed, ω_{sm}, and the torque balance is given as

$$\tau_t = \tau_e + D_d\omega_{sm} \quad \text{or} \quad \tau_m = \tau_t - D_d\omega_{sm} = \tau_e \tag{2.2}$$

where τ_m is the mechanical shaft torque. If the mechanical torque, τ_m, is greater than the electrical torque, τ_e, the rotor will accelerate. On the other hand, if τ_e is greater than τ_m the rotor decelerates. The rotor velocity can be expressed by

$$\omega_m = \omega_{sm} + \Delta\omega_{sm} = \omega_{sm} + \frac{d\delta_m}{dt} \tag{2.3}$$

where δ_m is the rotor angle in mechanical radians, and the derivative of the rotor angle is the speed deviation from synchronous speed given in mechanical rad/s. Substituting equation 2.3 into 2.1, gives the following equation:

$$J\frac{d^2\delta_m}{dt^2} + D_d\left(\omega_{sm} + \frac{d\delta_m}{dt}\right) = \tau_t - \tau_e \tag{2.4}$$

Substituting equation 2.2 into 2.4, the following equation is obtained.

$$J\frac{d^2\delta_m}{dt^2} + D_d\frac{d\delta_m}{dt} = \tau_m - \tau_e \tag{2.5}$$

Multiplying with the synchronous speed, ω_{sm}, using the fact that $P = \tau\omega$, and approximate that $\omega_m = \omega_{sm}$ during a disturbance, equation 2.5 can be rewritten as

$$J\omega_{sm}\frac{d^2\delta_m}{dt^2} + \omega_{sm}D_d\frac{d\delta_m}{dt} = P_m - P_e \tag{2.6}$$

The inertia constant, H, is defined as

$$H = \frac{0.5J\omega_{sm}^2}{S_n} \tag{2.7}$$

The damping coefficient is expressed as: $D_m = D_d\omega_d$. The mechanical power angle and angular speed is replaced with electrical radians and electrical radians per second. Equation 2.6 can now be expressed as

$$\frac{2HS_n}{\omega_s}\frac{d^2\delta}{dt^2} + D_m\frac{d\delta}{dt} = P_m - P_e \tag{2.8}$$

The damping term is replaced with P_D, and the equation is converted into a per unit representation [9]. The speed deviation in electrical rad/s is given by the time derivative of the rotor angle,

meaning $d\delta/dt = \Delta\omega = \omega - \omega_s$. The second-order differential equation is further represented as two first-order equations:

$$2H\frac{d\omega}{dt} = P_m - P_e - P_D \tag{2.9}$$

$$\frac{d\delta}{dt} = \omega_N\omega = (2\pi f_N)\omega \tag{2.10}$$

Together, equation 2.9 and equation 2.10 represent the electromechanical dynamics of a synchronous machine, and are fundamentally important when studying the frequency response of a power system.

2.4 Automatic Generation Control

The operation of automatic generation control (AGC) is fundamental in determining the frequency response after a load change. Large and slow changes are handled centrally, by determining at regular intervals which generating units will be operating. The small and fast load changes, however, are dealt with by AGC. AGC has several tasks, but this thesis will focus on AGC as frequency control.

2.4.1 Generation Characteristic and Droop

The relationship between valve position and mechanical power is assumed to be linear, so that the idealized turbine power-speed characteristic can be described as

$$\frac{\Delta\omega}{\omega_n} = -\rho\frac{\Delta P_m}{P_n} \tag{2.11}$$

where P_n is the rated capacity of the generator, and ΔP_m is the corresponding additional power output due to a change in speed, $\Delta\omega$. ω_n is the rated speed and ρ is referred to as the the droop for the generating unit. Since rotational speed is proportional to frequency, equation 2.11 may be rewritten as

$$\frac{\Delta f}{f_n} = -\rho \frac{\Delta P_m}{P_n} \quad \text{or} \quad \frac{\Delta P_m}{P_n} = -K \frac{\Delta f}{f_n} \tag{2.12}$$

where $K = 1/\rho$ is the effective gain of the governing system, Δf is the frequency change which leads to an additional power output and f_n is the rated frequency of the power system (50 Hz in the Nordic system).

By rearranging equation 2.12, the following expression for the droop is obtained:

$$\rho = -\frac{\Delta f / f_n}{\Delta P_m / P_n} \tag{2.13}$$

Physically the droop can be interpreted as the percentage change in speed required to move the valves from fully open to fully closed [1]. The concept of droop control is applied in governing systems to ensure that load changes only result in small frequency changes. A small droop setting will result in small frequency changes, but the droop cannot be zero or negative. In a large interconnected power system, the total generation characteristic is found by adding the change in mechanical power output for each generator during steady state, where all generators operate at the same frequency.

$$\Delta P_T = \sum_{i=1}^{N_G} \Delta P_{mi} = -\frac{\Delta f}{f_n} \sum_{i=1}^{N_G} K_i P_{ni} = -\Delta f \sum_{i=1}^{N_G} \frac{K_i P_{ni}}{f_n} \tag{2.14}$$

where N_G is the number of generators in the system. Figure 2.1 shows how the speed-droop characteristic of two individual generators are added according to equation 2.14, to obtain the equivalent generation characteristic. A power system's ability to compensate for a power imbalance is defined by this characteristic. A large power system will have close to a horizontal generation characteristic, which means that a large imbalance will lead to a relatively small frequency change. This is one of the great advantages of an interconnected power system.

Figure 2.1 is somewhat simplified, as it assumes a linear characteristic over the full range of power and frequency variations. Every turbine will in practice have a technical limit, either thermal or mechanical depending on the technology utilized. The constraint is a maximum power output, P_{max}, which the turbine cannot override. If the system frequency drops while the tur-

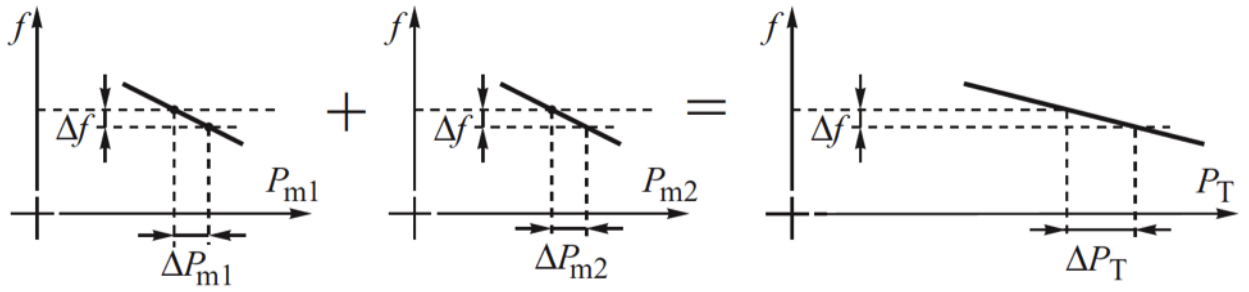

Figure 2.1: Summation of the speed-droop characteristic of two generating units [1].

bine is operating at this point, it will not result in a further increase of mechanical power for this particular turbine. Its speed-droop characteristic will become a vertical line, where $\rho = \infty$. The equivalent generation characteristic of the system will be given by the number of units operating away from their maximum limit, the spinning reserve [1].

2.4.2 Spinning Reserve

The amount of spinning reserve is the difference between the sum of the ratings of all operating units and their actual load [1].

$$r = \frac{\sum_{i=1}^{N_G} P_{ni} - P_L}{P_L} \tag{2.15}$$

In equation 2.15, r is the spinning reserve coefficient, and describes the relative difference between maximum capacity of the system and the actual system load. The spinning reserve gives information on how well a power system can handle large disturbances. It can be shown that a smaller spinning reserve coefficient, r, gives a bigger drop in frequency when there is a loss of power in the power system. This is due to the fact that spinning reserve is not assigned equally throughout the system, leading to a non-linear generation characteristic. When the power system is large and composed of a large number of operating units (such as the Nordic one), the generation characteristic will be composed of many small sections with different slopes. For every section that reaches its maximum limit, the slope will become steeper until there is no spinning reserve left and the droop is infinite. Figure 2.2 shows an approximation of what a static system generation characteristic could look like.

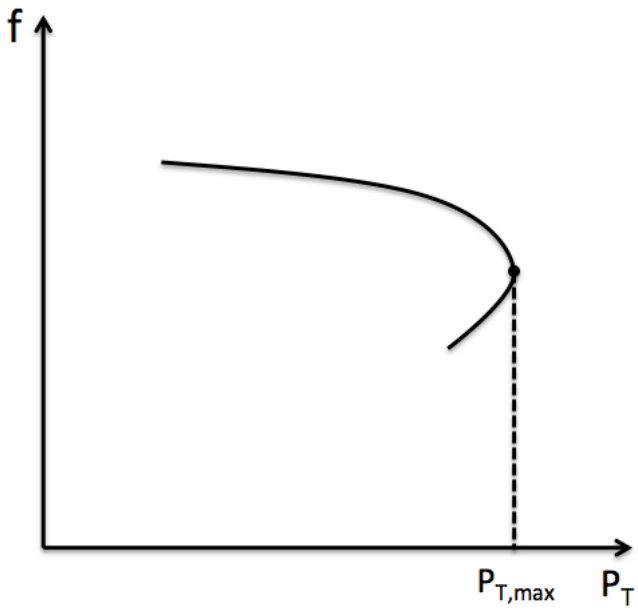

Figure 2.2: Example of a power system generation characteristic.

2.4.3 Primary Control

Primary frequency control is performed by the turbine governors and is activated when the frequency changes while the reference values of regulators are kept constant. When load demand increases and the frequency drops, two things will happen; a reduction of demand due to frequency sensitive loads, ΔP_L, and an increase of generation, ΔP_T, due to the action of the turbine governors. The change in frequency dependent loads is relatively small, $\Delta P_T >> \Delta P_L$. Primary control is the first action of defense against disturbances and can only be activated if there is more spinning reserve left in the system. It is critical to avoid a large drop in frequency or in the extreme case; frequency collapse. To avoid such an event, spinning reserve should be uniformly distributed in the power system. Each subsystem should ensure a large enough spinning reserve proportional to its share in the overall energy production. This is referred to as the solidarity principle. If a large disturbance occurs, and all the primary reserves are located in another part of the network, transmission lines could be overloaded and the disturbance could spread to the rest of the system. Requirements for primary control, such as the solidarity principle, are present to avoid problems like this. Other requirements include droop settings and how fast the reserves should be able to activate [1]. The specific requirements for primary frequency control in the Nordic power system are described further in section 2.6.

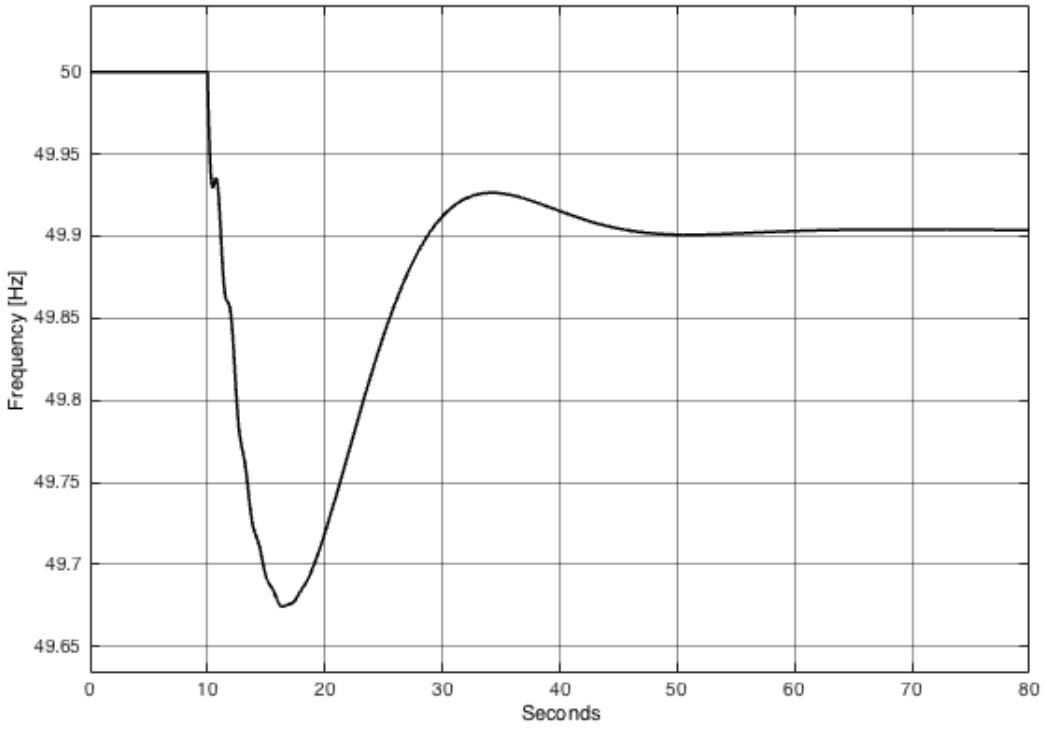

Figure 2.3: Power system frequency response after a disturbance.

2.5 Power System Frequency Response

As described previously in this chapter, if there is a connection (or disconnection) of a large load or if a generator is suddenly tripped by protection equipment, the power produced by the turbines and the power consumed by the loads will be unequal for a longer period of time. This long-term distortion in the power balance will initially be covered by the kinetic energy of the rotating masses in the system. As a result, the frequency of the system will drop. This change of frequency is divided into four stages. Each stage and its corresponding dynamics will be briefly explained. A more thorough explanation is provided in [1]. An illustration of a typical frequency response can be seen in Figure 2.3.

2.5.1 Stage I - Rotor Swings in the Generators

This stage lasts for the first few seconds of an under-frequency event and can be understood by applying the equal area criterion. For simplification a second-order model (the classical model) of a synchronous generator is used. The power-angle characteristic of the model is shown in

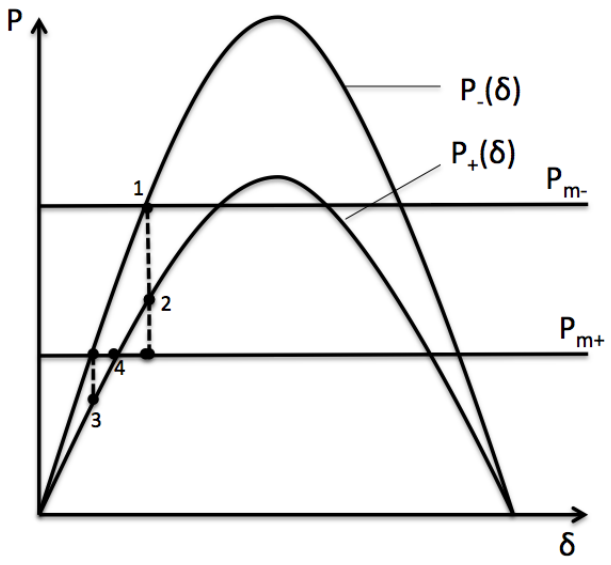

Figure 2.4: The equal area criterion determintes the first stage of the frequency response.

Figure 2.4. The generator has an operating point and is in steady state. A disturbance, such as tripping of a generator, will change the power-angle characteristic, leading to a new operating point. Since the rotor angle can not change immediately, the electric power of the generator will be greater than the mechanical power delivered by the prime mover. According to the swing equation, this will make the rotor lose kinetic energy and start decelerating. Due to its momentum, the rotor will decelerate past the new operating point. The mechanical power is now greater than the electrical power, and the rotor will start accelerating again. The oscillations will eventually be damped out. These rotor swings will have a greater amplitude for the local generators than for the other generators in the system. During stage I, the speed of the machines will therefore be different and the instantaneous frequency at each generator bus will be different. Another important aspect of this stage is that the contribution of each generator in meeting load demand will depend on its electrical distance from the disturbance.

2.5.2 Stage II - Frequency Change

The situation previously described can only last a few seconds before the other generators in the system start to slow down due to the power imbalance. Hence, the system frequency will drop and stage II begins. The time span of this stage is from a few seconds to several seconds. If

all the generators remain in synchronism, they will slow down at approximately the same rate. The rate of frequency decline will be governed by the system inertia. The contribution of each generator in meeting the power imbalance is solely dependent on its inertia. It can be shown that the power contribution is proportional to its own inertia, given by

$$\Delta P_{lII} = \frac{M_l}{M_l + M_s}\Delta P_0 \quad \text{and} \quad \Delta P_{sII} = \frac{M_s}{M_l + M_s}\Delta P_0 \tag{2.16}$$

where the subscript l represents the local generator, the subscript s represents the rest of the system and the subscript II indicates that this equation is valid in stage II. ΔP_0 is the lost generation or the additional load, while the constant M is defined as

$$M = \frac{2HS_n}{\omega_s} \tag{2.17}$$

2.5.3 Stage III - Primary Control by the Turbine Governing Systems

Stage III has a time span of several seconds and depends on how the generating units and loads react to the frequency drop. Figure 2.5 gives an illustration of how the intersection between the load characteristic, P_L, and the static turbine characteristic, P_T, determines the operating frequency. The figure shows how the load demand will have a small change if the frequency changes. When a generating unit is lost, the turbine characteristic will change and the new operating point will be the intersection of P_L and P_{T+}, where P_{T+} is the turbine characteristic after the disturbance. Due to the time constants of the turbine and the governor, this point can not be reached instantaneously. Because the power mismatch is initially large, as described in previous stages, the frequency will drop. The governors will utilize droop control and increase the turbine's mechanical output. The aforementioned time constants will cause the frequency to drop beneath the power trajectory, $f(P_T)$, until a local minimum, the frequency nadir, is reached and the frequency starts to rise. How low this point lies is determined by load damping and the effectiveness of governor action. Droop control will drive the frequency restoration up from the frequency nadir, and past the new operating point, again due to the time constants. Eventually the oscillations are damped and the frequency settles at the point of intersection between P_L and P_{T+}.

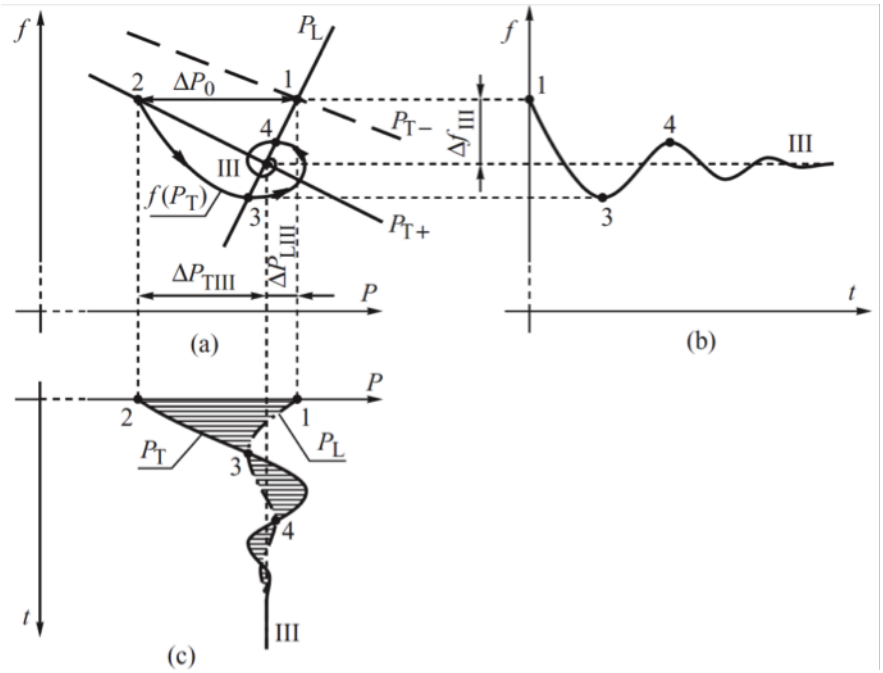

Figure 2.5: Parameters during stage 3: a) the generation characteristic and frequency response characteristic; b) frequency over the time span; c) changes in power [1]

2.5.4 Stage IV - Secondary Control by the Central Regulators

In the last stage secondary control (or central AGC) is activated, with the purpose of covering the remaining power imbalance in the system and returning the frequency to its nominal value. Stage IV has a time span of seconds to minutes. The stage will last until the frequency is restored, or all the available regulating power is activated. If more regulating power is needed, the transmission system operator (TSO) must verbally instruct other generating units to increase their power output, so that the remaining imbalance is made up for. Secondary control is not a part of this thesis and will thus not be further discussed.

2.6 Ancillary Services

Ancillary services are by definition of [10] "some operational reserved services procured by the Transmission System Operator (TSO) for keeping a balance between supply and demand, stabilizing the transmission system and maintaining the power quality on an economical basis in any competitive electricity market environment." Examples of services included in this term

are voltage control, blackstart capability and grid loss compensation. This thesis focuses on frequency control, or more precisely frequency containment reserve (FCR).

FCR, or what is previously described in this thesis as primary control, is a part of a control system that deals with the momentary balance between production and consumption [11]. As previously discussed, FCR activates automatically if an imbalance causes the system frequency to change. Having access to enough reserve capacity, and that the reserves give the expected response, is fundamentally important to maintain a safe operation of the power system [12]. In the Nordic system the FCR is divided into FCR-N and FCR-D. FCR-N is used during normal operating conditions or small load variations, while FCR-D is used during disturbances.

2.6.1 FCR-N

FCR-N is a symmetric reserve and will be automatically activated if the frequency varies within the area of 49.9 – 50.1 Hz. The reserves should be regulated out within 2 – 3 minutes. The total capacity of FCR-N in the Nordic system is today at 600 MW, which fulfills the requirement of the TSO. 210 MW of this capacity is located in Norway. To avoid congestion on transmission lines and the disturbance spreading throughout the network, each subsystem is required to have 2/3 of its own FCR-N. It is important that a subsystem can be self-sufficient and work in islanded operation until the disturbance is cleared. Other than that, the service can be power exchanges between the subsystems. Both Norway and Sweden use exclusively hydropower as FCR-N, which is reflected in the model developed in this thesis [3, 13].

2.6.2 FCR-D

FCR-D is a continuation of FCR-N, because it activates when the frequency drops below 49.9 Hz. This type of reserve is not symmetric, and only contributes during events that cause a frequency drop. General requirements for FCR-D, set by the TSO, includes [3, 13]:

- The reserves should activate at 49.9 Hz and be fully activated at 49.5 Hz.
- The total amount of FCR-D should be able to prevent the frequency from dropping below

49.5 Hz following a dimensioning fault.[1]

- Activation of FCR-D should not create other problems in the power system.
- Each subsystem should be able to supply 2/3 of its FCR-D itself.

FCR-D has the same requirement as FCR-N on a subsystem's share in the reserve capacity, due to the reasons mentioned. Even though the total capacity of FCR-D in the Nordic system is at 1200 MW (Norway's share is around 350 MW), a large disturbance could cause the frequency to drop below 49.5 Hz [12]. In the case of such an event, the following requirements must be met [3]:

- 50 % of the FCR-D should be activated within 5 seconds.
- 100 % of the FCR-D should be activated within 30 seconds.

2.7 DC Power Flow

The reasons for using a DC power flow is often the fact that it has linear properties, is non-iterative while also reliable. Its simplicity results in a considerable analytical and computational advantage. A DC model is limited to active power-oriented applications, where the effects of network voltage and reactive power conditions are minimal [14]. This is often a difficult criterion to judge, but since frequency analysis is related to the active power balance, a DC power flow is chosen as appropriate for this study.

An AC power flow solution can be found by the following set of equations, if the complex voltages at every bus are known:

[1] According to [3], dimensioning faults are "faults which entail the loss of individual major components (production units, lines, transformers, bus bars, consumption etc.) and entail the greatest impact upon the power system from all fault events that have been taken into account."

$$Y = \begin{bmatrix} y_{11} & \dots & -y_{1j} & \dots & -y_{1n} \\ \vdots & \ddots & & & \vdots \\ -y_{i1} & \dots & y_{ij} & \dots & -y_{in} \\ \vdots & & & \ddots & \vdots \\ -y_{n1} & \dots & -y_{nj} & \dots & y_{nn} \end{bmatrix} \tag{2.18}$$

$$y_{ij} = |y_{ij}|\angle\theta_{ij} \tag{2.19}$$

$$V_i = |V_i|\angle\delta_i \tag{2.20}$$

$$V_j = |V_j|\angle\delta_j \tag{2.21}$$

$$P_i = \sum_{j=1}^{n} |V_i||V_j||y_{ij}|cos(\delta_i - \delta_j - \theta_{ij}) \tag{2.22}$$

$$Q_i = \sum_{j=1}^{n} |V_i||V_j||y_{ij}|sin(\delta_i - \delta_j - \theta_{ij}) \tag{2.23}$$

where n is the number of busbars and the indices i and j represent the ith and jth busbar respectively. Y is the admittance matrix, which contains both the magnitudes, $|y_{ij}|$, and the angles, θ_{ij}, of the Y matrix elements. The complex voltage at bus i consists of a voltage magnitude, $|V_i|$, and a voltage angle δ_i. The same goes for bus j and every bus in the system. P_i and Q_i are the active and reactive power at bus i.

The following simplifications are made to the previous equations, to derive the DC power flow equations:

- Grid losses are assumed to be zero, or incorporated into the loads. This assumption can only be applied to the high voltage transmission grid, which is the grid under study in this thesis. The reactances dominate the resistances in such a grid ($x_i >> r_i$) and the resistances are therefore neglected. The impedances are now purely imaginary, which means that the angle of the admittance matrix elements will be $\theta_{ij} = -\frac{\pi}{2}$ for diagonal elements and $+\frac{\pi}{2}$ for off-diagonal elements.

- The voltages at each bus are assumed uniform and close to the nominal voltage, i.e. all

voltage magnitudes are assumed to be 1.0 p.u.

By applying these approximations to equation 2.22, and using the fact that $cos(x-\pi/2) = sin(x)$, the equation for active power becomes

$$P_i = \sum_{j=1}^{n} |y_{ij}| sin(\delta_i - \delta_j) \tag{2.24}$$

A final approximation is that the difference between the voltage angles is small, leading to a linearization of the sine and cosine functions:

$$sin(\delta) = \delta \quad \text{and} \quad cos(\delta) = 1.0 \tag{2.25}$$

which leads to a final set of linear equations

$$P_i = \sum_{j=1}^{n} |y_{ij}| (\delta_i - \delta_j) \tag{2.26}$$

The same assumptions can be applied to the equations of reactive power, but this is not relevant in this thesis. The active power in the transmission lines is calculated as

$$P_{i-j} = |y_{ij}| (\delta_i - \delta_j) \tag{2.27}$$

where P_{i-j} is the active power flow between bus i and j [15].

2.8 Per Unit System

The main quantities of interest in power system analysis are power, voltage, current and impedance. It is common practice to express these as decimal fractions of corresponding base quantities. The advantage of such a system is that the different voltage levels for elements like generators, transformers and lines disappear, and the network is reduced to a system of simple impedances. The per-unit value of any quantity is defined as:

$$\text{p.u. value of a quantity} = \frac{\text{Actual value}}{\text{Base value}} \tag{2.28}$$

The actual value and the base value (or reference value) have the same unit, which means that the per-unit value is dimensionless. The equation is valid for any unit. Base values for all the four main quantities are defined according to the equations below, to create a complete per-unit system.

$$S_{pu} = \frac{S}{S_B} \qquad V_{pu} = \frac{V}{V_B} \qquad I_{pu} = \frac{I}{I_B} \qquad Z_{pu} = \frac{Z}{Z_B} \tag{2.29}$$

All calculations in this thesis are done in per-unit, as the system greatly simplifies these calculations [16, 17].

Chapter 3

Method

In order to uncover the power system impact of variable-speed hydro, a simulation model was constructed. The software of choice and the method of modeling are described in this chapter. The chapter describes how the different power systems are modeled and what assumptions and simplifications are made. The specific elements and the details of the model are described in chapter 4. The main model of this thesis is what is referred to as the DC model. Another model, the AC model, was developed to verify that some of the assumptions made in the main model are fair.

3.1 Software

The software of choice for this thesis was MATLAB® and Simulink®, which are both developed by MathWorks®. MATLAB®, or matrix laboratory, is a programming platform designed specifically for engineers and scientists. The matrix-based programming language is today used by over one million engineers and scientists worldwide [18]. Simulink® is a graphical block diagram platform, which is used together with MATLAB® to design a system in a simulation environment [19]. The combination of the two programs make up a powerful tool for simulation and control of dynamic systems, which makes them a suitable choice to help fulfill the objectives of this thesis.

MATLAB® was used to set values and perform calculations for the model developed in Simulink®.

Only blocks from the standard library are used in the model, such as transfer function blocks, integrators, steps, constants, gains, MATLAB® function blocks etc. Scopes were used to graphically represent the response of several variables of interest.

3.2 Method of Modeling - DC Model

The system model is built based on a combination of a hydropower plant model, the swing equation and DC power flow, created with inspiration from [20]. A simplified model of a VSC is also present to enable variable speed operation of a hydropower plant. All function blocks are presented in detail in chapter 4. The advantages of this method of modeling are that the model can be easily scaled without making too many changes, and a short simulation time without many long and complicated calculations. The model uses per unit values, where the system frequency is 50 Hz and the global base value for apparent power, S_{base}, is 1000 MVA. Each generating unit has its own local base value, M_{base}, related to the capacity of the generator. The model is linearized around an initial operating point, meaning all parameter values are given as deviations from this point. For example, a frequency of -1 Hz will equal 49 Hz. The system under study is a representation of some of the different bidding zones or areas in the Nordic power system. Each area consists of one single generating unit, representing the total capacity in the area, and a load.

3.2.1 Loads and Generating Units

The loads are modeled as unit step blocks. A step in demand is used to approximate the loss of a generator, since the frequency response will follow the same stages in both situations. A sudden disconnection of a HVDC link is also simplified in this way. The generating unit is modeled as a synchronous generator connected to a hydropower plant turbine and governor. The generating unit can also be scaled down to represent a single generator connected to a bus and be part of a smaller grid. In this way the model can be used to study the effects of variable speed hydro, both on small and large grids. The variable-speed plants are modeled as negative loads on the load buses, so the power produced by the variable-speed plant will immediately reduce the load at that bus. Non-synchronous production, such as solar- and wind power, are also

modeled as negative loads on the load buses, although these types of energy sources are not specifically present in the model. However, an increase in their production leads to a reduction in synchronous capacity.

3.2.2 DC Power Flow

The output of each area and their accumulated generators are the generator voltage angles. The angles are, together with the load changes and admittance matrix of the system, used as input variables to a MATLAB® function block, which computes the DC power flow. The output is the amount of electric power, ΔP_e, each generator must increase or decrease its production with, in order to handle a load change. The change in electric power is then used as a feedback loop to the corresponding generator. The DC power flow function block calculates the electric power by the expression $P_e = Y\delta$. Expressed in matrix form, the equation becomes:

$$\begin{bmatrix} \Delta P_{e,1} \\ \vdots \\ \Delta P_{e,n} \\ -\Delta P_{l,1} \\ \vdots \\ -\Delta P_{l,m} \end{bmatrix} = \begin{bmatrix} Y_{11} & Y_{12} \\ Y_{21} & Y_{22} \end{bmatrix} \begin{bmatrix} \Delta\delta_{g,1} \\ \vdots \\ \Delta\delta_{g,n} \\ \Delta\delta_{l,1} \\ \vdots \\ \Delta\delta_{l,m} \end{bmatrix} \tag{3.1}$$

where the ΔP_e's represent the change in electric power of the generators and the ΔP_l's represent the change in power loads. Y_{11}, Y_{12}, Y_{21} and Y_{22} are submatrices of the admittance matrix Y, the $\Delta\delta_g$'s are changes in the generator voltage angles and the $\Delta\delta_l$'s are the changes in the voltage angles between the buses. Here, generation is defined as positive power, while consumption is defined as negative power. Equation 3.1 can be compressed to

$$\begin{bmatrix} \Delta P_e \\ -\Delta P_l \end{bmatrix} = \begin{bmatrix} Y_{11} & Y_{12} \\ Y_{21} & Y_{22} \end{bmatrix} \begin{bmatrix} \Delta\delta_g \\ \Delta\delta_l \end{bmatrix} \tag{3.2}$$

The generator voltage angles are input variables, while the admittance matrix and load values are known quantities. The remaining voltage angles and the electric power output can be calcu-

lated as follows:

$$\Delta\delta_l = Y_{22}^{-1}(-\Delta P_l - Y_{21}\Delta\delta_g) \tag{3.3}$$

$$\Delta P_e = Y_{11}\Delta\delta_g + Y_{12}\Delta\delta_l \tag{3.4}$$

The calculated ΔP_e's are multiplied with the global base value, S_{base}, and divided by the local base value, $M_{base,i}$, so the correct per unit values are given to the generators through a feedback loop. As the changes in voltage angles between busbars, $\Delta\delta_l$, are calculated, the changes in line power flow are easily obtained. Equation 3.5 shows how the aforementioned angles can be used, together with the admittances of the lines, to calculate the change in DC power flow. The example grid is the same one used in the test-case in chapter 4, and can be seen in Figure 4.6.

$$\begin{bmatrix} \Delta P_{1-2} \\ \Delta P_{1-3} \\ \Delta P_{3-4} \end{bmatrix} = \begin{bmatrix} -y_{12} & y_{12} & 0 & 0 \\ -y_{13} & 0 & y_{13} & 0 \\ 0 & 0 & -y_{34} & y_{34} \end{bmatrix} \begin{bmatrix} \Delta\delta_1 \\ \Delta\delta_2 \\ \Delta\delta_3 \\ \Delta\delta_4 \end{bmatrix} \tag{3.5}$$

Finally, it should be mentioned that DC power flow is only applicable on high voltage lines, so the model should be limited to analyzing high voltage transmission grids.

3.2.3 Frequency

As this method does not take into account voltages and currents, the electric frequency is not defined. The frequency can, however, be modeled from the speed of the generators, since this is a synchronous system. The electric frequency can be modeled as a nominal speed, ω_N. The speed of generators with large inertia will be of higher significance than that of smaller units. Thus, the frequency is defined in the model as a scaled mean value of the sum of the generator speeds. For a system with n generators, ω_N is given as:

$$\omega_N = \frac{\sum_{i=1}^{n} \omega_i H_i}{\sum_{i=1}^{n} H_i} \tag{3.6}$$

ω_N is given as an input variable to the generating units. Together with the individual generator speed, ω_i, the frequency dependent load of each generator is determined. This frequency

dependent load will not contribute when the system is in steady state, because the generator speed is equal to the system frequency. Because of the way the frequency is modeled, an area cannot consist of only variable-speed hydro. These plants are not directly connected to the grid and their rotor's rotating speed will not be equal to the grid frequency. During the simulations, each area must therefore have a certain amount of normal hydro capacity to prevent the system from becoming unstable.

3.2.4 Voltage Source Converter

The VSC, which controls the power output of the variable-speed plants, is connected to a load bus behind a reactance and a small resistance. The VSC is modeled as the inner current control loop of the modulus optimum control algorithm, as described in chapter 4. As the objectives are to improve frequency stability in under-frequency events, a back-to-back VSC is not necessary. A single VSC is grid connected, where the DC voltage control is assumed ideal for simplicity.

3.3 Method of Modeling - AC Model

In order to verify the model's behaviour and its ability to approximate a power system, an AC model is used for comparison. The AC model, which was developed in a master thesis at NTNU [21], originally aims at improving rotor angle stability by utilizing synthetic inertia from wind farms. The wind farm is replaced by a hydropower plant, but the converter controlling the power output is kept with its original tuning. By performing simple adjustments, the model can be used to show the impact variable-speed hydro has on a small system. The major differences that separate the DC- and the AC model will here be explained. For further understanding of the methods used in the AC model, please see [21].

3.3.1 Loads and Generating Units

The synchronous generators of the AC model are of fifth-order, meaning that each generator has five state variables that are taken into account when describing the system. The state variables are generally internal emf, rotor speed and angular displacement from the reference machine.

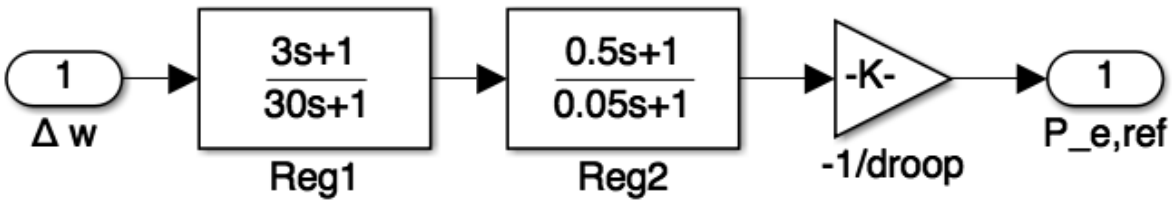

Figure 3.1: Transfer function that imitates a governor response, with $\Delta\omega$ as input variable and $P_{e,ref}$ as output variable.

The DC model only represents the generators as a second-order model. The result is fewer state variables and a shorter simulation time. The turbine and turbine governor of the two models are the same, but an AVR is included in the AC model, as voltage control is necessary for a model that includes subtransient emfs. For the variable-speed plant a VSC controls the power output. A transfer function, given in Figure 3.1, is added to the VSC model in order to imitate the governor response. This simplification is performed in order to not alter the code too much. The same transfer function is used for the plant in the DC model, so the two models are comparable. The transfer function for imitating a governor response, was found in the previous project work [22].

As mentioned, the loads of the DC model are modeled as unit step blocks which represent the variable ΔP_l. For the AC model, impedance loads are used. This means that the loads are represented as impedances in the admittance matrix, and the power they consume is calculated with help of the bus voltage.

3.3.2 Algebraic Equations of the Dynamic Simulation

The two models work under the same principle, by using numerical integration in order to solve a set of differential equations and find the value of the state variables. A script performing algebraic equations are used to find the necessary variables so that the differential equations can be solved using numerical integration. DC power flow equations are used for the DC model, while Figure 3.2 shows the flowchart for the method used in the AC model. The state variables first need to be related to the system reference frame where the q-axis of a chosen generator serves as reference. When all variables are in the same reference frame, the current injection model

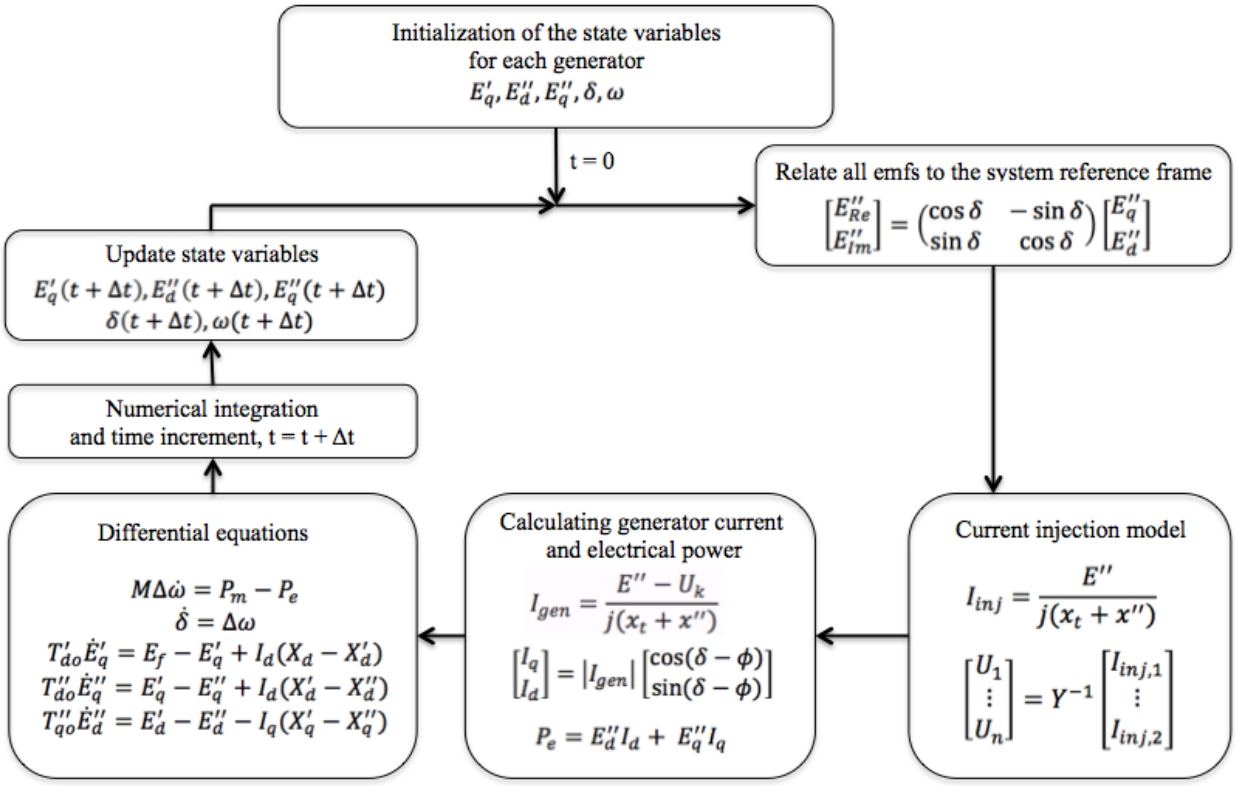

Figure 3.2: Flowchart of the dynamic simulations.

can calculate all the bus voltages. The final step is to calculate the d- and q-axis generator current and the electric power of each generator. These three variables, together with the terminal bus voltage, are used in a feedback loop to the generator model. The frequency is estimated and used in the same way as in the DC model.

3.3.3 Voltage Source Converter

The VSC is modeled as an emf behind a transformer reactance. Switching dynamics of the inverter are neglected and since the entire AC model is in the dq-frame, so is the inverter. Hence, the need for a phase lock loop is not present and the control scheme is different from that of a real inverter. The converter takes as input the terminal voltage, voltage angle referred to the system reference and the d- and q-axis currents. The AC model inverter controls both the active power and the voltage, while the DC model inverter only controls active power.

Chapter 4

Model

Parts of this chapter are redrafts of [22], since this thesis is a continuation of that project work. To illustrate the benefits of variable-speed hydro, a grid model, representing a large part of the Nordic grid, was developed in Simulink®. All elements of the model are described in the following sections, as well as the network for the test case and the Nordic power system. For a detailed block diagram of the entire model, see Appendix B.

4.1 Turbine and Turbine Governor

To represent the turbine and turbine governor of a hydropower plant, a model developed in [23] is used. The model's parameter values are taken from [24]. The paper aims at identifying turbine and turbine governor dynamics using PMU measurements, and also performing theoretical val-

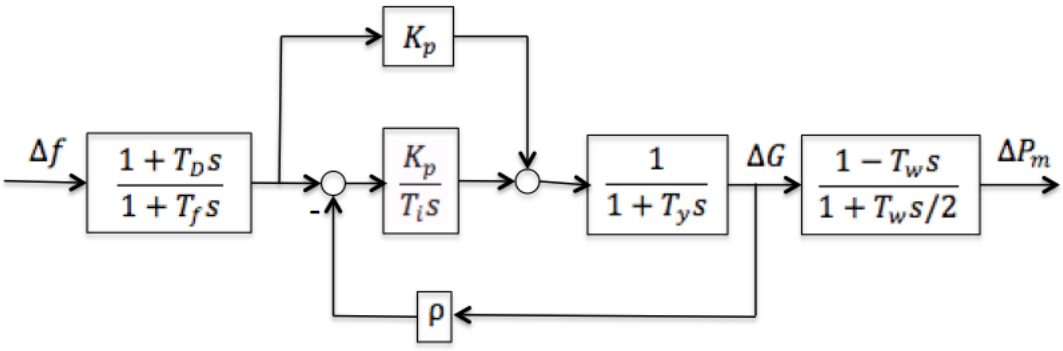

Figure 4.1: Hydro turbine governor and turbine block diagram

Table 4.1: Parameters used for the turbine and turbine governor model in Figure 4.1

Variable	Explanation	Value
T_D	Derivative time	0
T_f	Low pass filter time constant	0
K_p	PI controller gain	1.5
T_i	PI integral time	5s
ρ	Droop	0.1
T_y	Servo time constant	0.2s
T_w	Water starting time	1.01s

idation using DC power flow. A block diagram of the turbine and turbine governor is shown in Figure 4.1, while the parameters used are presented in Table 4.1.

4.2 Electromechanical Dynamics

The swing equation, presented in chapter 2, is used to model the electromechanical dynamics of the power plant. This is referred to as the classical model, or the second-order model, because it contains two state variables. The classical model is often the model of choice for simplified power system analysis. It represents the synchronous generator as a constant emf, E', behind a transient reactance, X'_d. The model assumes very small changes in the d-axis armature current and the excitation voltage during transients. By linearizing around an initial operating point,

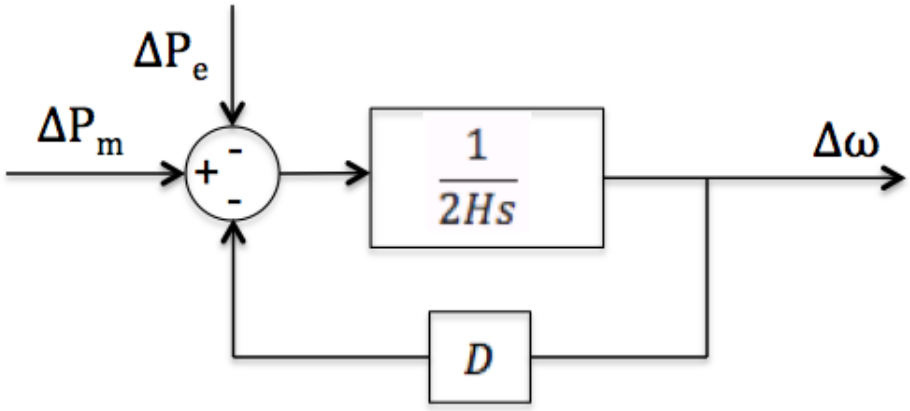

Figure 4.2: Block diagram of the electromechanical dynamics

the two equations for the state variables are

$$\begin{aligned} 2H\Delta\omega &= \Delta P_m - \Delta P_e - D\Delta\omega \\ \frac{d\Delta\delta}{dt} &= 2\pi f \Delta\omega \end{aligned} \tag{4.1}$$

The second equation is not relevant for the variable-speed plant, since it is not directly connected to the grid. A block diagram of the modeled electromechanical dynamics is shown in Figure 4.2.

4.3 Voltage Source Converter

The reported main advantage of variable-speed hydro is the ability to control power in pump mode [4, 5]. A back-to-back voltage source converter is required to perform this service. This thesis utilizes only one VSC and can thus only enable variable-speed in generation mode. Hence, pump mode is disregarded in this thesis. This section provides a brief explanation of the configuration, modeling and tuning of the VSC. A more thorough explanation is given in the previous project work [22].

4.3.1 Configuration

A three-phase two-level VSC is the choice of converter in this thesis, due to its simplicity. It is a six pulse bridge equipped with self-commutating switches (IGBTs). The configuration is shown in Figure 4.3. The variables and parameters are

V_{abc} = Grid AC voltage in all three phases
R = Resistive component of the line impedance
L = Inductive component of the line impedance
$V_{conv,abc}$ = Average converter voltage for the three phases
V_{dc} = DC-link voltage

If the switching dynamics are ignored and we assume a close to sinusoidal voltage, Kirchoff's

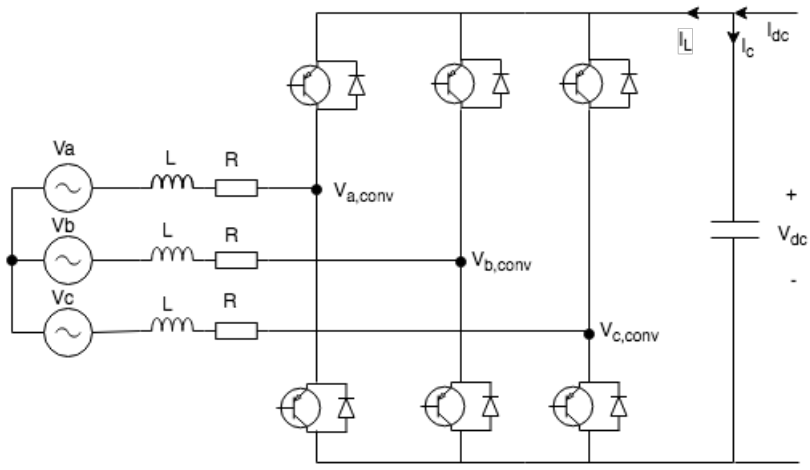

Figure 4.3: Configuration of a grid-side voltage source converter.

voltage law gives the following equation for the three phases.

$$v_{abc} = Ri_{abc} + L\frac{d}{dt}i_{abc} + v_{conv,abc} \tag{4.2}$$

A DQ transformation, or Park transformation, is applied in order to perform control in DC rather than in AC. The benefits are an easier control scheme and the fact that an integrator in the controller will eliminate steady state error between a time invariant signal and the reference. Equation 4.2 in the rotating dq-frame becomes

$$\begin{aligned} v_d &= Ri_d + L\frac{d}{dt}i_d - \omega Li_q + v_{conv,d} \\ v_q &= Ri_q + L\frac{d}{dt}i_q + \omega Li_d + v_{conv,q} \end{aligned} \tag{4.3}$$

A coupling between the two axes is introduced in the transformation, which will have to be taken into account when performing control. It can be shown that power in the dq-frame is expressed as

$$\begin{aligned} P &= \frac{3}{2}(v_d i_d + v_q i_q) \\ Q &= \frac{3}{2}(-v_d i_q + v_q i_d) \end{aligned} \tag{4.4}$$

The d-axis is then aligned with the grid voltage, meaning $v_q = 0$, and the power relationships become

$$\begin{aligned} P &= \frac{3}{2} v_d i_d \\ Q &= -\frac{3}{2} v_d i_q \end{aligned} \tag{4.5}$$

Active and reactive power can thus be controlled independently by adjusting the d- and q-axis currents.

4.3.2 Modeling and the Vector Control Principle

The vector control principle is the most common way of controlling a simple VSC. The control scheme is illustrated in Figure 4.4. Since voltages are not present in the model, and active power is the main variable of interest in frequency analysis, the VSC is simplified to only include the inner current controller. Active power is controlled by controlling the d-axis current, and the signal is sent as a change in electric power, ΔP_e, to the swing equation. The model of the VSC is shown in Figure 4.5. The controller is a simple PI-controller, the converter is represented as a small time delay due to computational time and switching, and the system transfer function is found from equation 4.3. The cross coupling term is seen as a disturbance, and is handled by a

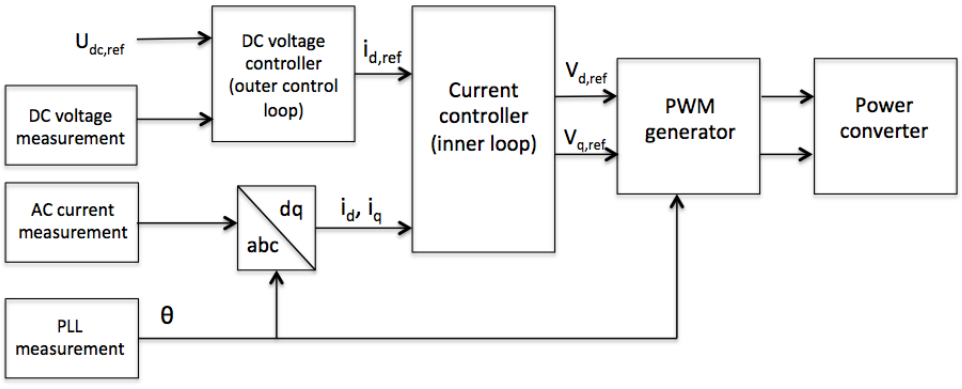

Figure 4.4: The vector control principle scheme.

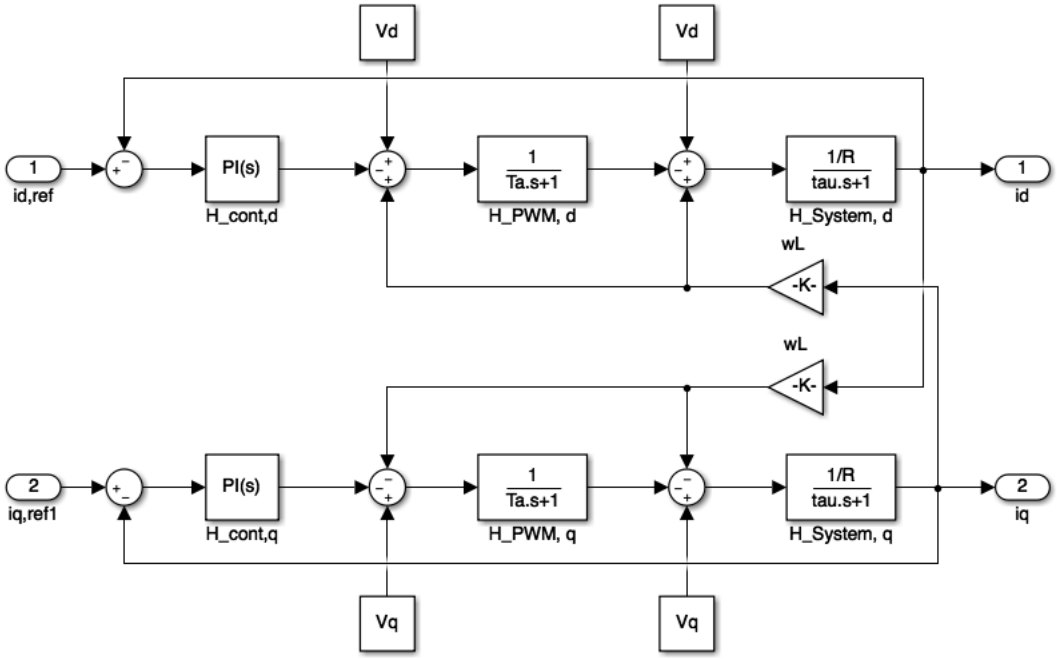

Figure 4.5: Simplified model of a voltage source converter.

voltage feed-forward compensation. The three transfer functions are

$$H_{cont,dq} = K_p \frac{1+T_i s}{T_i s} \quad , \quad H_{PWM,dq} = \frac{1}{1+\tau_a s} \quad , \quad H_{sys,dq} = \frac{1/R}{1+\tau s} \tag{4.6}$$

where K_p and T_i are the tuning variables, τ_a is a time delay and τ is a time constant equal to $\frac{L}{\omega_b R}$ in per unit. ω_b is the synchronous speed $2\pi f$. The modulus optimum is used to tune the controller, leading to

$$\begin{aligned} K_p &= \frac{\tau R}{2\tau_a} \\ T_i = \tau &= \frac{L}{\omega_b R} \end{aligned} \tag{4.7}$$

The system parameter values and the tuned control parameter values are found in Appendix D. The VSC's step response has a settling time of 21 ms [22]. The DC voltage control is normally about 10 times slower than the inner current control, but the response is still considered close to instantaneous compared to the slow electromechanical dynamics.

4.4 MATLAB® Function Blocks

The model contains two MATLAB® function blocks: the network calculations and the frequency calculation. Both will be described in the following subsections.

4.4.1 Network Calculations

The network calculation function block runs the DC power flow equations, as described in section 3.2.2. The input variables are the difference in the voltage angles from the generators, the change in the loads and the admittance matrix of the system. The line admittance matrix is also taken as input, so that the line power flows can be calculated. All the changes in voltage angles are gathered in a common vector, while the load changes are placed in another vector. Equation 3.3 and 3.4 can now calculate the remaining voltage angles and the electric power outputs, the $\Delta P_{e,i}$'s. The electric power outputs are fed back to the generators and the dynamic simulation runs the next time step. The line power flows are not further used in the model, but are calculated so that it is possible to study whether some of the lines are overloaded during a disturbance.

4.4.2 Frequency Calculation

The modeled frequency, or nominal speed, is calculated as the scaled mean value of the sum of the generator speeds. The frequency function block takes as input the individual speeds, ω_i, of all generators without variable speed feature, and the normalized inertia constants, H_i. The calculated of the output frequency, ω_N, is expressed in equation 3.6.

4.5 Test Case Network

The test case used to validate the model is the base case used in [21]. The topology is a two-area system, each with two generators, where the areas are separated by a 250 km transmission line. The topology is illustrated in Figure 4.6. The capacity of each generator is as follows: G1 = 4000 MW, G2 = 600 MW, G3 = 4800 MW, G4 = 600 MW. Generator 2 is a hydropower plant with variable-speed feature, represented by an inverter in the aforementioned figure. The other

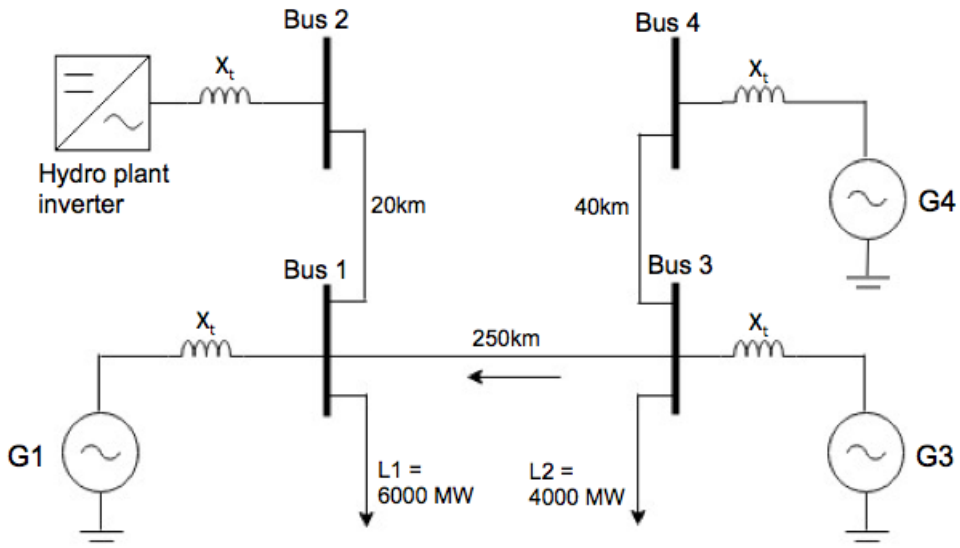

Figure 4.6: Test case network.

generators are normal operating hydro plants with a droop setting of 12 %. The voltages and the injected apparent power at each bus for the test case operating point are given in [21]. Since variable-speed plants are modeled as a negative load at a generator bus, Bus 2 is not present in the DC model test case. The variable-speed plant has to be connected to Bus 1, but since the line is only 20 km long and Bus 2 has no other connections, this is a fair approximation.

4.6 Nordic Power System Network

Further, the DC model is scaled up to represent parts of the Nordic power system, in order to study the power system impact of variable-speed hydro. Which areas are included and the connections between them are illustrated in Figure 4.7. The model could easily represent the total Nordic grid, but the network presented was found sufficient to highlight the advantages of variable-speed hydro. The model comprises eight bidding zones, each consisting of a generator, with a transient d-axis reactance, and a load. The values of these reactances are given in Table B.1. The reactances of the transmission lines are chosen as the inverse of the maximum transfer capacity. The transfer capacities were found in [25], and their values, along with the line reactance values, are given in Table B.2. The admittance matrix of the system is given in Appendix C. As previously mentioned, variable-speed plants are modeled as negative loads at the

load buses. The placement of the variable-speed plants and their respective capacities varies throughout the thesis' case studies, and the plants are therefore not present in Figure 4.7. In which areas the variable-speed plants are located, and their capacities, are specified for each case. Non-synchronous generation, such as solar- and wind power, are also modeled as negative loads on the load buses. They are not specifically present in the model, but the local capacity of the hydropower plant is reduced with the same amount of power as the renewable generation at that moment. The local base value, or capacity, of each area is set from the production at a specific hour. The production is assumed to be 80 % of the total capacity online, meaning $C = P/0.8$, where C is the capacity and P is the production. Production data is gathered from Nord Pool [26]. There is no limit for the available spinning reserve in any of the areas. Each area will contribute according to its respective capacity and droop setting.

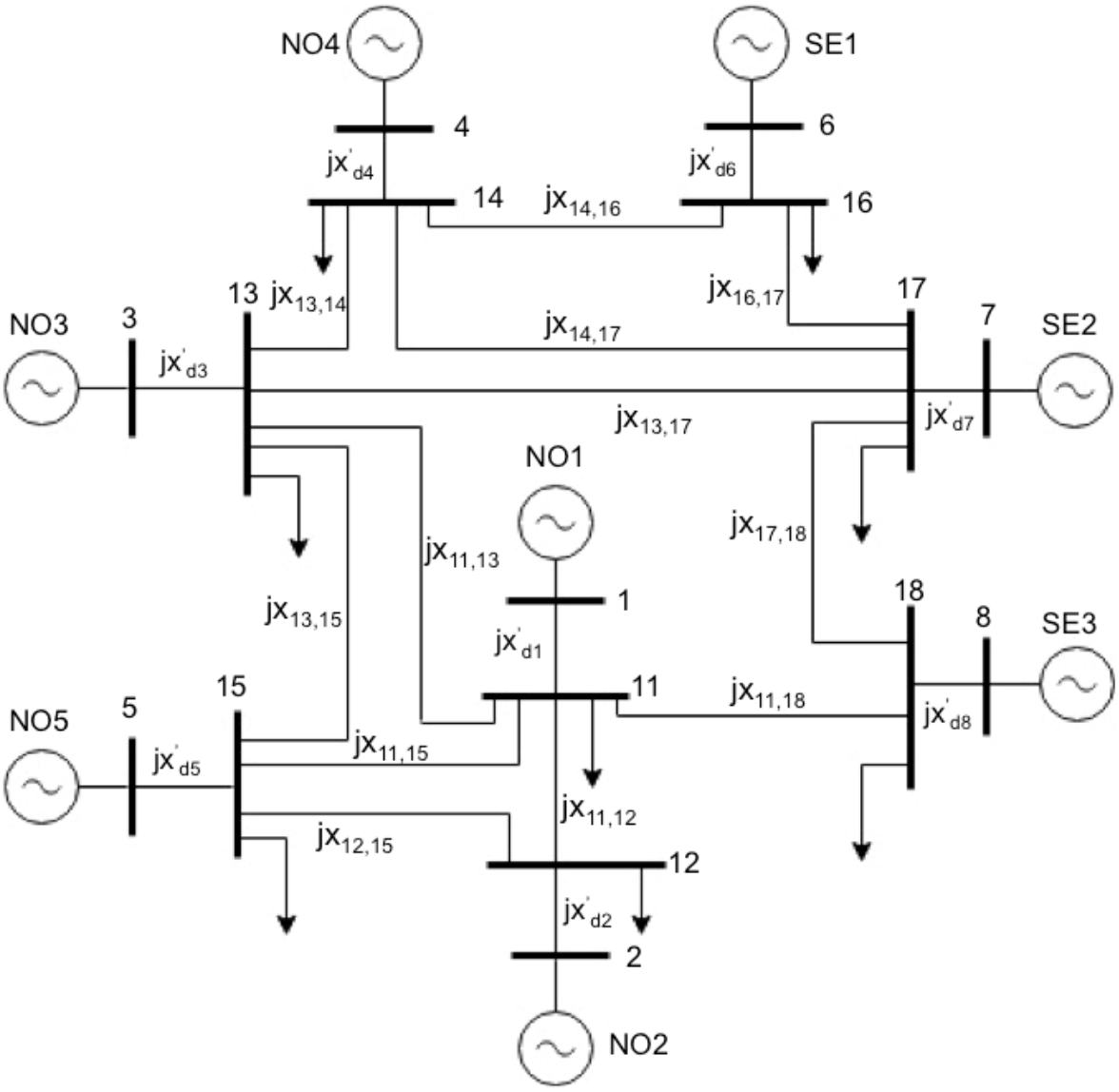

Figure 4.7: The Nordic grid including NO1, NO2, NO3, NO4, NO5, SE1, SE2 and SE3. Each area has a droop of 12 % except SE3, which has a droop of 50 % to approximate the mix of hydropower and nuclear power in that area.

Chapter 5

Simulations and Results

5.1 Validation

The validation of the main model is done by comparing it to an AC model in the test case scenario described in section 4.5. A load of 500 MW is suddenly connected at bus 1. The two models are tested both with and without variable-speed feature. For the case where the plant at bus 2 does not run with variable speed, the transfer function shown in Figure 3.1 is added to both the DC- and the AC model to imitate the governor response. By this simplification, the code is not altered too much and the response is close to a realistic hydropower plant. The transfer function was found, and the comparison to a grid-connected plant was done, in [22].

Both models have the same system parameters, including inertia constants, turbine- and governor settings, and are subjected to the same operating condition. One variable will be compared at a time. Each variable is compared twice, once with- and once without variable-speed feature. The graph to the left represents the system with only normal hydropower, and the one to the right has a variable-speed plant. The DC model is always represented by the red curve, while the AC model has a blue curve.

Validation of the DC model is also done by scaling it up to represent parts of the Nordic grid, and analyzing if the model behaves according to the theory presented in chapter 2. The frequency of each area will be compared to the stages of the power system frequency response, with focus

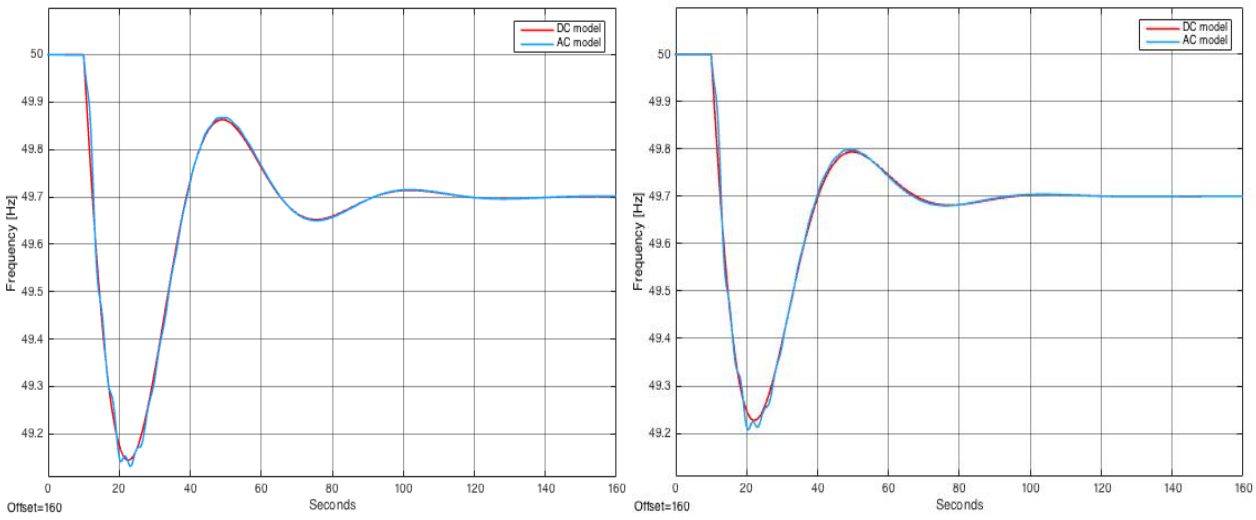

(a) Without VSH

(b) With a VSH plant at bus 2

Figure 5.1: System frequency response after a load step of 500 MW at bus 1.

on the first three stages. The electric power of each generator will also be under study, to see if there are any weaknesses in the plant model.

5.1.1 Frequency

The frequency drops, which can be seen in Figure 5.1, are similar in the two models, both in the case with variable-speed hydro and the one without. The frequencies in the two models follow each other closely, with some fluctuations in the AC model. This is a result of the load modeling. The difference in the load change is shown in Figure 5.2. As the load in the AC model is an impedance load, it is voltage dependent and will oscillate with the same frequency as the voltage. This is more realistic, although the voltage controller could probably be tuned more precisely. However, voltage control is not in the scope of this thesis, and better tuning would lead to a smaller amplitude of the oscillations and a response closer to the DC model.

5.1.2 Electrical and Mechanical Power

The electric power output of the generator at bus 2 is the variable with the largest deviations, see Figure 5.3. The AC model has an aggressive transient behaviour, while the DC model avoids this. This is the case for both the normal- and the variable-speed plant, due to the simplification

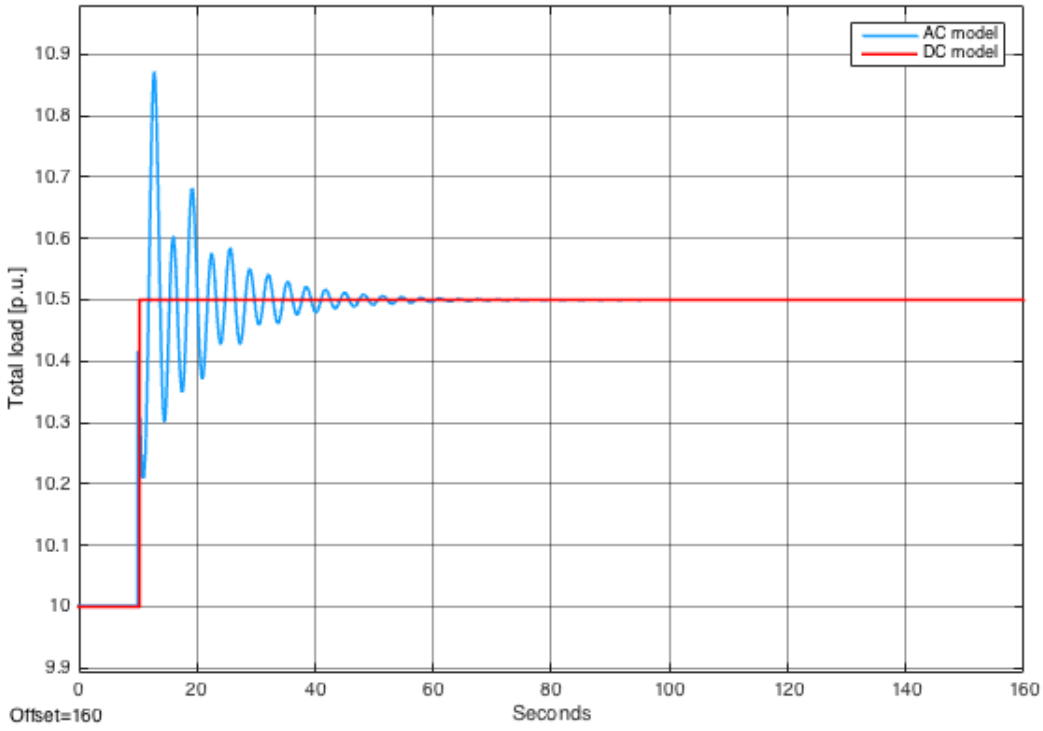

Figure 5.2: Load change

that a VSC is controlling the power and imitating the governor response. The explanation for the transient behaviour is the control of the VSC. The DC model is tuned according to the modulus optimum and the power is controlled with frequency as the reference signal. The AC model, however, is tuned for a specific case study [21]. The power is a function of the bus voltage, which fluctuates and causes large oscillations in the power output before the voltage control of the VSC corrects them. The transient is damped out in about one second, and the responses of the two models are similar for the rest of the time span. The AC model's power output varies more than that of the DC model over the time span, due to the oscillating load change as previously described.

The two large generators in the system, generators 1 and 3, produced some oscillations in the electrical power output. The electrical power output of generator 3 is shown in Figure 5.4. Generator 1 has a similar response. The two models both oscillate, but with different frequencies. The reason for the oscillations in the AC model is again poor voltage control. The frequency of the oscillations coincides with the voltage oscillations. The VSC was able to adjust quickly for

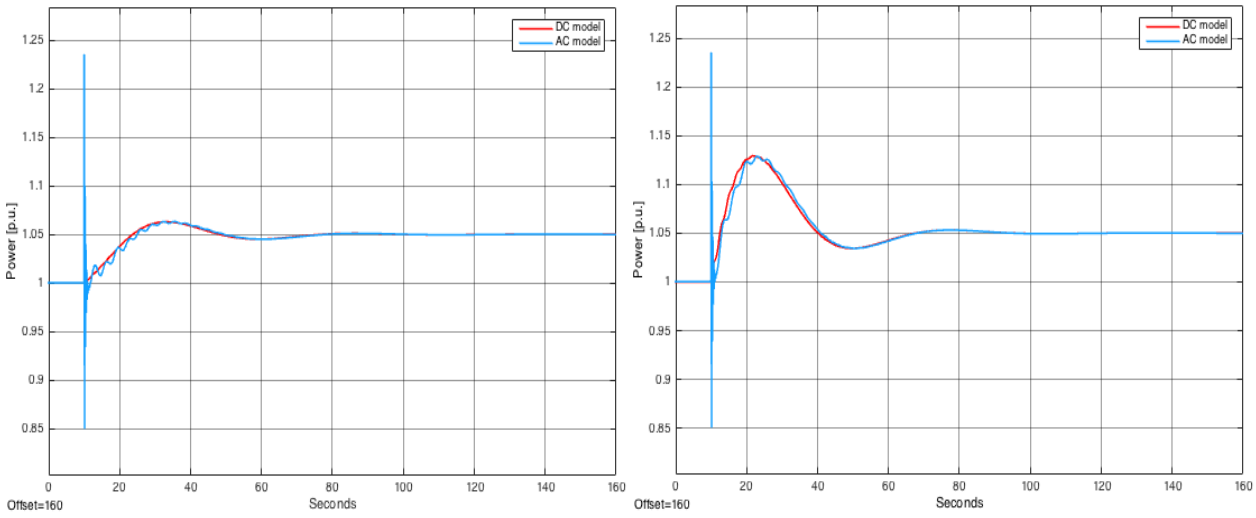

(a) Without VSH

(b) With a VSH plant at bus 2

Figure 5.3: Electrical power, P_e, of the generator at bus 2 after a 500 MW load increase at bus 1.

generator 2, but for a normal operating hydropower plant the AVR performs voltage control. The tuning of the AVR was done case specific in [21]. An optimal voltage response is not necessary for the comparison, therefore the AVR settings remain the same.

The electrical power output of the large generators in the DC model oscillates with a frequency that coincides with the voltage angles of the generators. A small grid, like this test case network, produces large and fast oscillations. The response of the large Nordic grid is studied in section 5.1.4. The frequency of the oscillations was somewhat decreased by increasing the transient reactance of the generators, but the damping was not significantly improved. The oscillations were damped out faster by increasing the damping term of each generator, but a large and unrealistic damping was not chosen.

The mechanical power of generator 1 is shown in Figure 5.5. All the other generators have similar responses. The two models are close to equal for this variable, because they have the same governor model. The difference in the number of state variables in the plant model affects the electrical power output, but not enough to discredit the DC model. The state variable of interest, the frequency, is close to identical in the two models. The deviation between the two models for the other presented variables has also been within reasonable limits. As the presented figures also show, the deviation between the two models does not change significantly by introducing

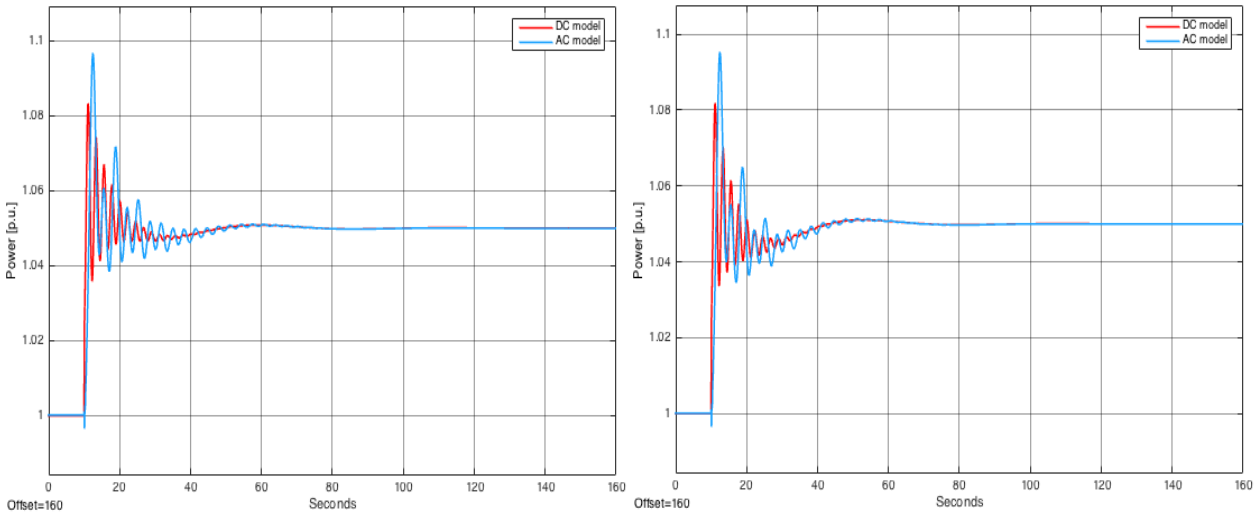

(a) Without VSH

(b) With a VSH plant at bus 2

Figure 5.4: Electrical power, P_e, of the generator at bus 3 after a 500 MW load increase at bus 1.

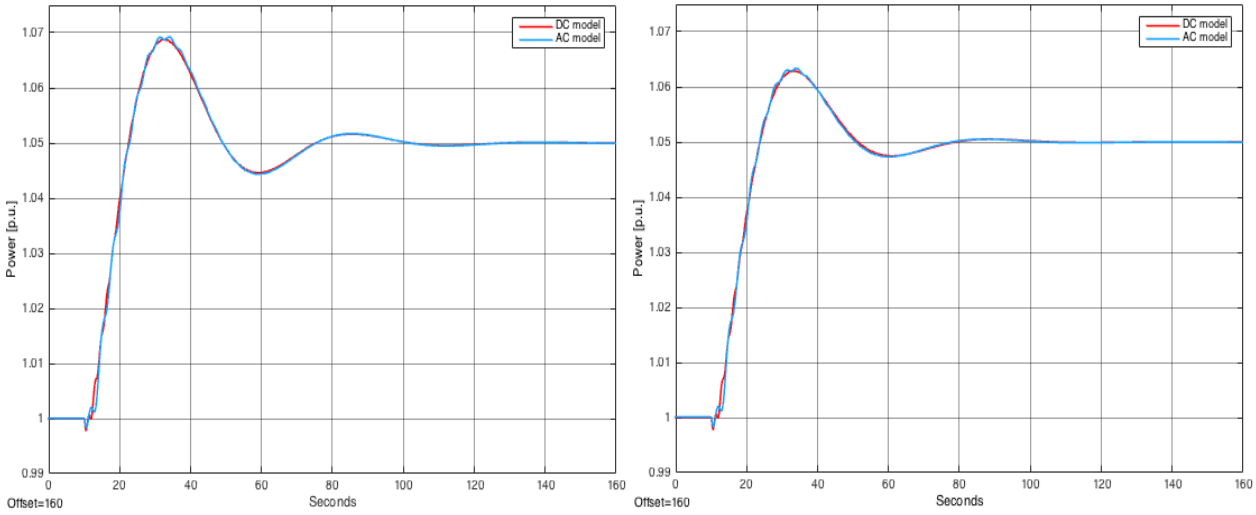

(a) Without VSH

(b) With a VSH plant at bus 2

Figure 5.5: Mechanical power, P_m, of the generator at bus 1 after a 500 MW load increase at bus 1.

Table 5.1: Base values for the Nordic power system test case.

Area	Normal hydro capacity [MVA]	Variable-speeed hydro capacity [MVA]
NO1	2000	0
NO2	4000	0
NO3	2000	0
NO4	3000	0
NO5	4000	0
SE1	3000	0
SE2	4000	0
SE3	8000	0

variable-speed hydro. The DC model thus seems appropriate to assess the power system impact for under-frequency events.

5.1.3 Comparison to Frequency Response Theory

Here, the network used by the DC model is the Nordic grid as illustrated in Figure 4.7. The base values for the test case are shown in Table 5.1. The disturbance is an additional load of 1000 MW in area NO1. The frequency of every area is shown in Figure 5.6. The entire trajectory of the frequency response, from drop to steady state, is given in a), while b) is zoomed in on the first few seconds of the drop.

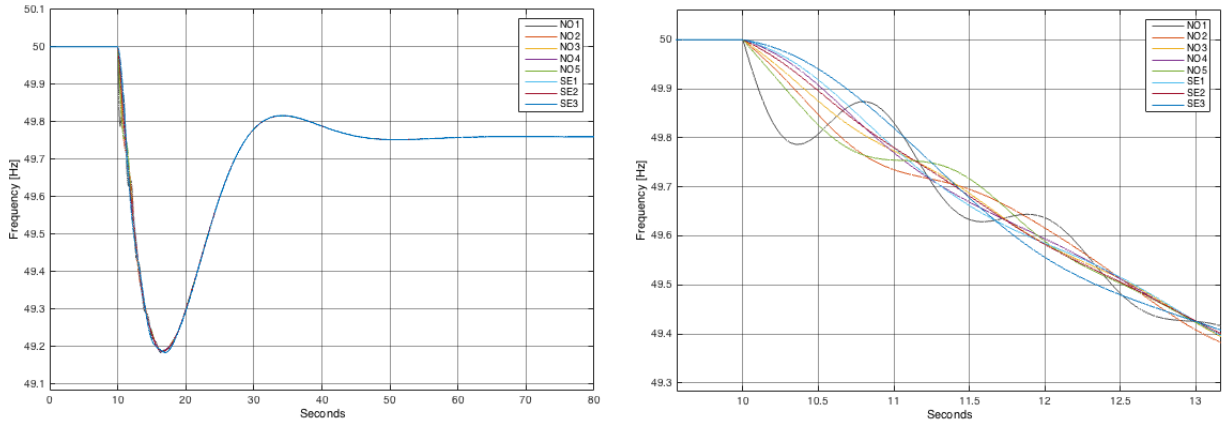

(a) The whole response

(b) The first few seconds

Figure 5.6: Frequency response of area NO1, NO2, NO3, NO4, NO5, SE1, SE2 and SE3 in the Nordic grid test case.

All the generators follow approximately the same response, with small deviations the first few seconds, also referred to as Stage I. The generators experience rotor swings due to imbalance between the electrical and mechanical power of the individual plant. After the disturbance, the rotor angle will oscillate around a new operating point until the oscillations eventually are damped out. The rotor swings will have a greater amplitude for local generators, which is evident in Figure 5.6 b), where the local frequency at NO1 drops first and has the largest rotor swings. This corresponds to the theory of Stage I, where the share of any given generator in meeting lost load will depend on its electrical distance from the disturbance. Therefore, the frequency of the adjacent areas NO5, NO2 and NO3 will drop faster and experience rotor swings greater than the other generators in the system farther from the disturbance. The area SE3 will not have the same swings because of a much greater inertia of the generator. The same characteristics were present when adding variable-speed hydro to the system. Hence, the model is consistent with the power system frequency response theory.

5.1.4 Change in Electrical Power

The generators in the system are all hydro-based and set with a droop of 12 %. The generation in area SE3, however, consists of a mix between hydropower and nuclear power. The accumulated generation in SE3 is therefore modeled as a hydropower plant, but with a droop setting of 50 %. This simplification may not be realistic, especially because nuclear power does not take part in primary control in the Nordic grid. The model is not taking this into account, which leads to an unrealistic contribution of electrical power during the first seconds after a disturbance. The droop setting makes the area's contribution to a disturbance reasonable in steady state, but the contribution during the frequency drop is far too high. The change in electric power for every area is shown in Figure 5.7. Both the base values and the disturbance are the same as in the frequency response test case. SE3 has a much larger change in power the first few seconds, because of its large inertia and capacity. The area SE3 is modeled this way for both the system with- and the system without variable-speed hydro. The comparison between a power system with- and a power system without variable-speed hydro will thus still be valid, even though the mix of hydropower and nuclear power in SE3 is simplified in this way.

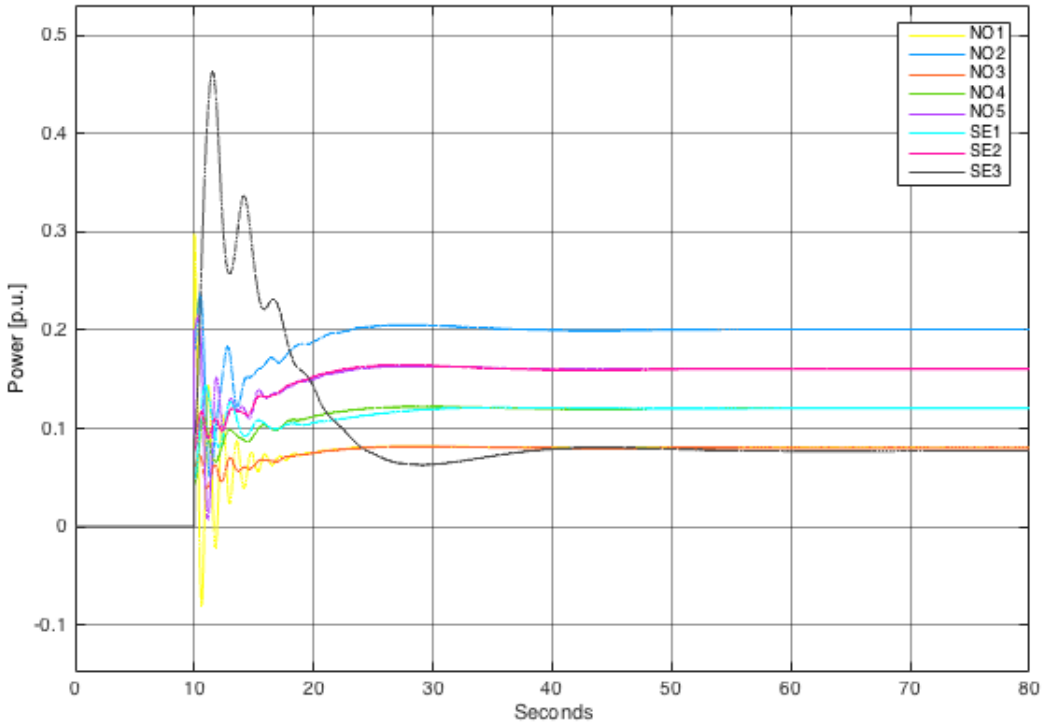

Figure 5.7: Change in electric power for all areas after a disturbance.

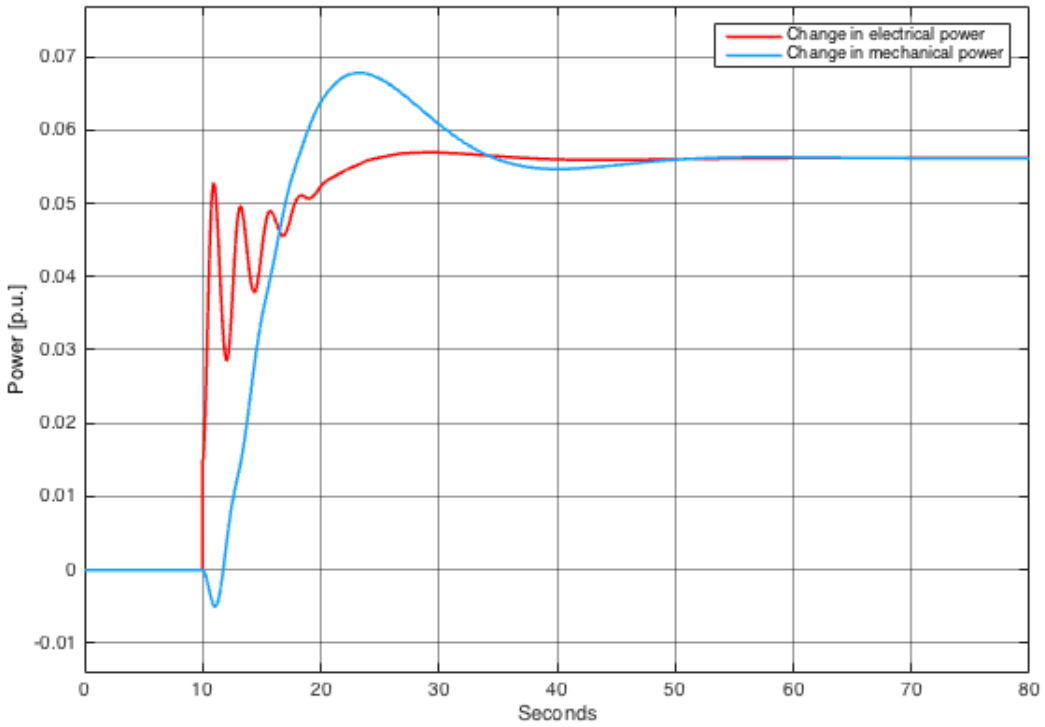

Figure 5.8: Change in electrical- and mechanical power for NO4 after a disturbance.

The small test grid produced fast oscillations in the electrical power output. The electrical power is a function of the rotor angle, and the generators in the test grid had large variations in rotor angle after the disturbance. The model representing the Nordic grid, which is larger and more interconnected, proved to be better equipped to handle a sudden load change. Figure 5.8 show the electrical and mechanical power of the accumulated generator in NO4. The other generators in the system have similar responses. The large and fast oscillations are no longer present due to the natural damping provided by the interconnected grid. A large and unrealistic damping term eliminated the oscillations for the test grid, but this was not necessary for the Nordic grid model. The main results are the simulations of the large Nordic grid, which gives a proper response in electrical power output. Therefore, a realistic damping term of the generators was chosen, and the oscillations in the test case were not further investigated.

5.2 Optimal Control of a Variable-Speed Plant

The VSC will act on the frequency deviation to adjust its power output. The droop control performed by the governors will decide how much each plant contributes in steady state after a disturbance. The control of the VSC is set the same way, meaning a stationary deviation in frequency gives a power reference according to the relationship given in equation 2.12. However, the goal is to find a control scheme that can limit the frequency drop, while also restoring the frequency to its steady state as fast as possible. Three different schemes are presented in Figure 5.9. The first one, Figure 5.9 a), is a simple proportional regulation or droop control as described earlier. Figure 5.9 b) adds a derivative term to set a higher power output reference during the frequency drop. At last, in Figure 5.9 c), a parallel control scheme with both a derivative- and an integral term is tested, in order to both limit the frequency drop as well as drive the frequency restoration.

The parallel control scheme proved to be the most effective in limiting the frequency drop and restoring the frequency, when tuned correctly. Figure 5.11 illustrates how the different control schemes, presented in Figure 5.9, perform during a disturbance. The base values for the system in this simulation are given in Table 5.2. The Bode plot for the suggested control scheme is given

Table 5.2: Base values for the Nordic power system test case.

Area	Normal hydro capacity [MVA]	Variable-speeed hydro capacity [MVA]
NO1	2000	0
NO2	4000	1000
NO3	2000	0
NO4	3000	0
NO5	4000	0
SE1	3000	0
SE2	4000	0
SE3	8000	0

in Figure 5.10. A longer derivative term led to a lower frequency drop, but the restoration acted slower. The integral term helped with the frequency restoration, and thus allowed for a longer active derivative term. The goal is to have the controller amplify the signal of the frequency drop and dampen the gain during frequency restoration. The challenge is that these frequencies are close to each other. Another challenge is the fact that the variable-speed plant aims to return to nominal speed as fast as possible. This is illustrated by Figure 5.12, which shows the speed deviation from nominal speed of the variable-speed plant. The graph shows how the plant reacts to the three different control schemes presented. The derivative action makes the plant

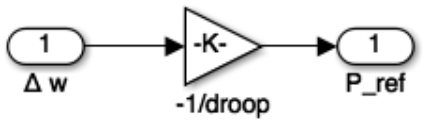

(a) Proportional regulation

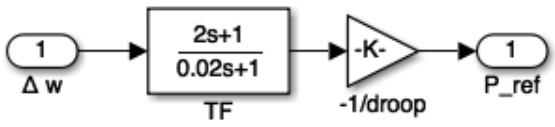

(b) Derivative term

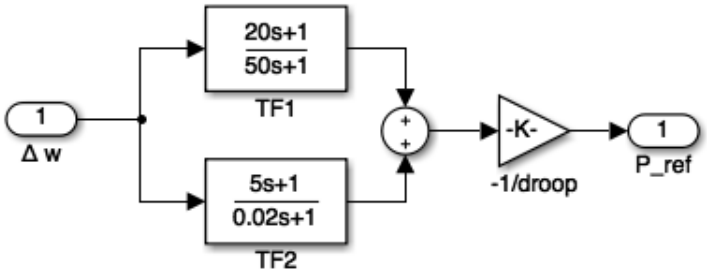

(c) Parallel control scheme

Figure 5.9: Control schemes of the model.

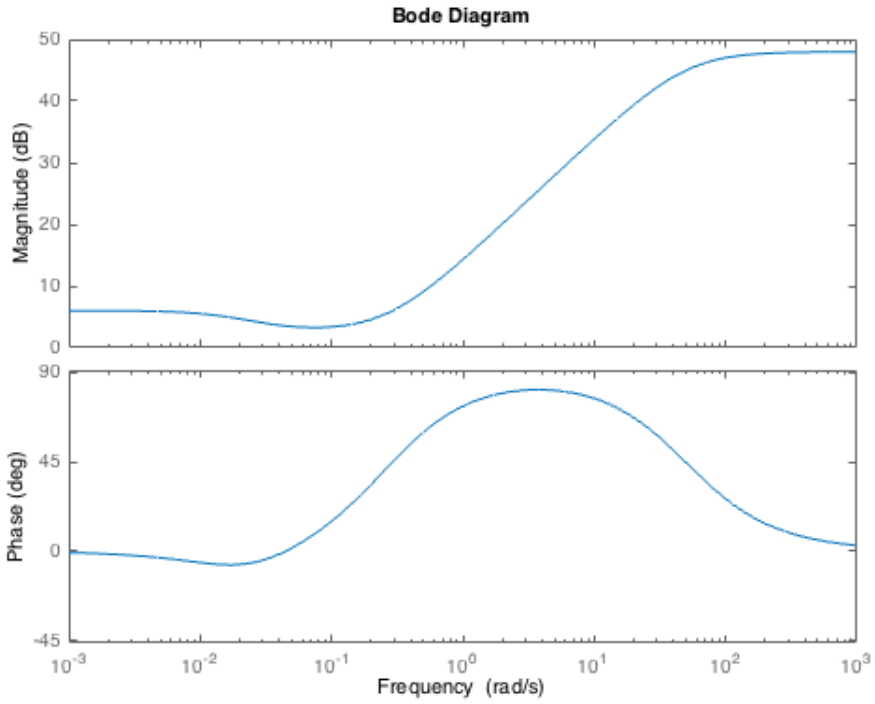

Figure 5.10: Bode plot of the suggested control scheme.

able to inject more active power to the grid during a disturbance, by releasing more kinetic energy and thus the rotor slows down. During the frequency restoration stage, however, the rotor will regain the kinetic energy it supplied during the frequency drop. The derivative action will make the plant regain kinetic energy faster during this stage. Also, due to the inertia of the rotating mass, the rotor will swing past the point of nominal speed and eventually be damped out. This is the reason why a normal hydro plant will drive the frequency to a higher level than the variable-speed plant can during the restoration stage, before the frequencies of both systems settle at approximately the same time. The steady state deviation from nominal frequency is somewhat smaller for the parallel control scheme, due to the presence of a summation block.

The suggested control scheme limits the frequency drop well, which is important for the frequency stability of the system. The suggested scheme is therefore used by all variable-speed hydro plants introduced later in this thesis, when assessing their impacts on the future power system.

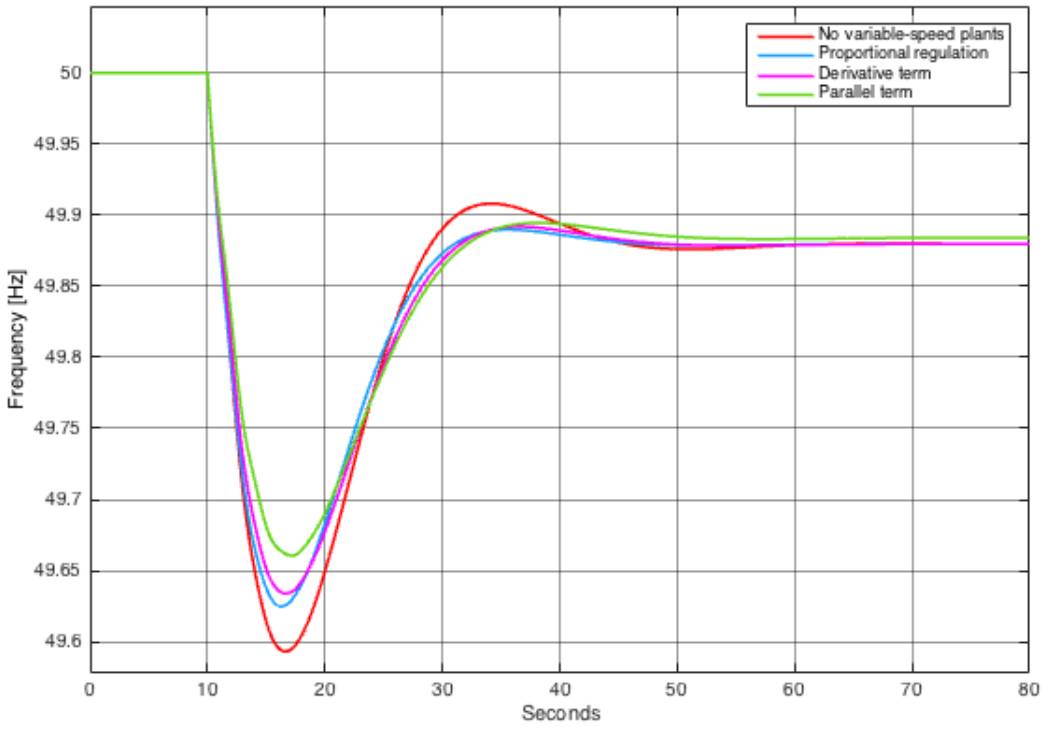

Figure 5.11: System frequency for the different control schemes with and without variable-speed hydro.

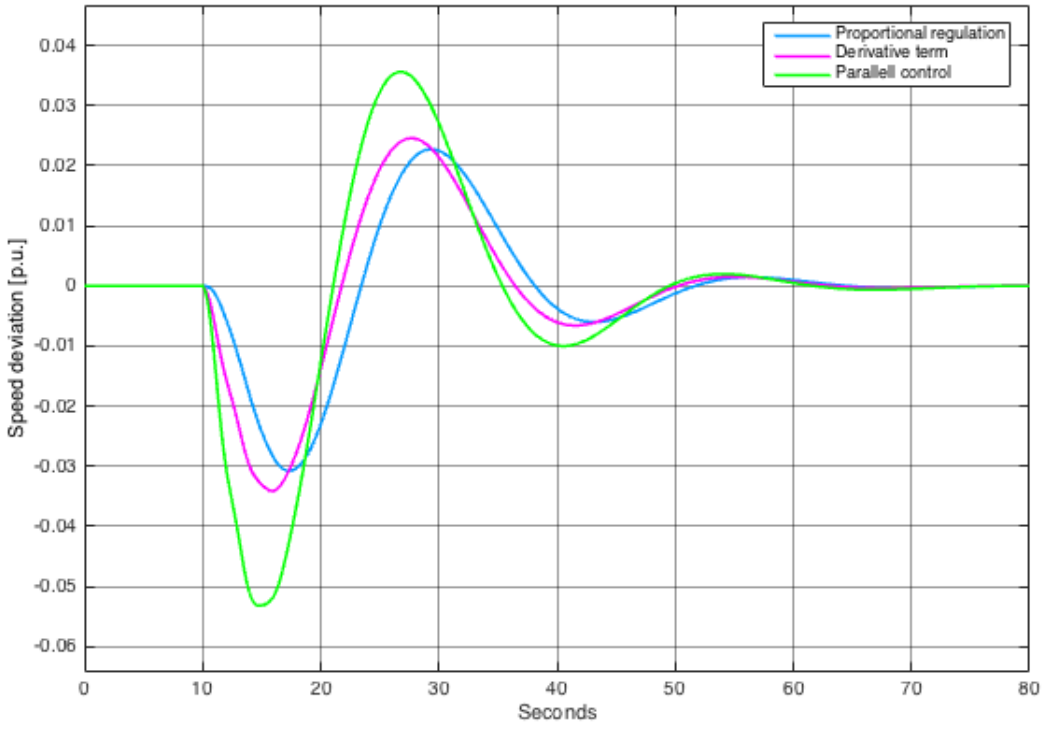

Figure 5.12: Deviation from nominal speed for the variable-speed rotor with different control schemes.

5.3 Variable-Speed Hydro in the Future Power System

There is a growing concern that the increase in renewable energy generation will lead to problems for the frequency stability in the future power system. Non-synchronous generation, such as solar- and wind power, does not contribute with spinning reserve. On a day where the sun shines and the wind blows, a smaller share of the generation will come from hydropower. Less spinning reserve will then be available, and frequency problems could occur. The previous section showed how properly tuned variable-speed hydro could help limit the frequency drop after a large disturbance. The Nordic power system of today does not contain any variable-speed hydro plants. This section will highlight and quantify the benefits of introducing variable-speed hydro to the Nordic grid. The simulation scenarios are built on real production data gathered from [26]. The data is taken from a summers day, when there are less rotational masses online, and the frequency is more fragile. The disturbances are chosen to be extreme, but are faults the network should be dimensioned for. The chosen disturbances are:

- Outage of a fully loaded HVDC cable: A 1400 MW load increase in NO2.
- Outage of the largest generating unit in Oskarshamn: A 1450 MW load increase in SE3.

The disturbances are in reality a drop in production, but a load step is chosen due to simplicity and its similar frequency response. First, today's grid is subjected to these disturbances. Second, assumptions are made to create grid scenarios for the Nordic network in 2040. Grids with different amounts of variable-speed hydro are compared to a grid without any VSH. The grids are all subjected to the disturbances mentioned.

5.3.1 Today's Situation

The 6^{th} of August 2017 between 12.00 - 13.00 is chosen as the time for the simulation of today's situation. The production at the time and the system base values are given in Table 5.3. An amount of 500 MW variable-speed hydro is introduced in NO2, to show how a relatively small amount of variable-speed capacity can bring benefits to today's system as well. The normal hydro capacity of NO2 will for that case be reduced by 500 MW.

Table 5.3: Production data and capacity base values for today's Nordic power system with no variable-speed hydro.

Area	Production [MW]	Normal hydro capacity [MVA]	Variable-speeed hydro capacity [MVA]
NO1	2249	2811	0
NO2	2707	3384	0
NO3	1680	2100	0
NO4	2504	3130	0
NO5	2597	3246	0
SE1	1353	1691	0
SE2	2883	3604	0
SE3	7726	9658	0

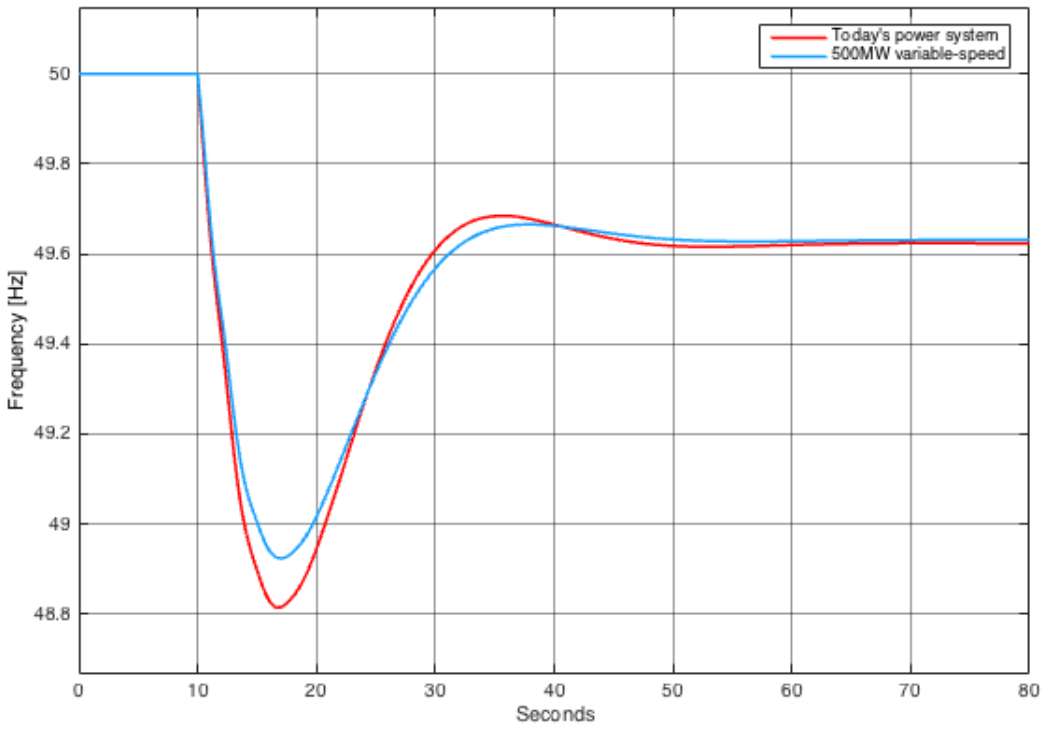

Figure 5.13: Frequency response after 1400 MW load step in NO2.

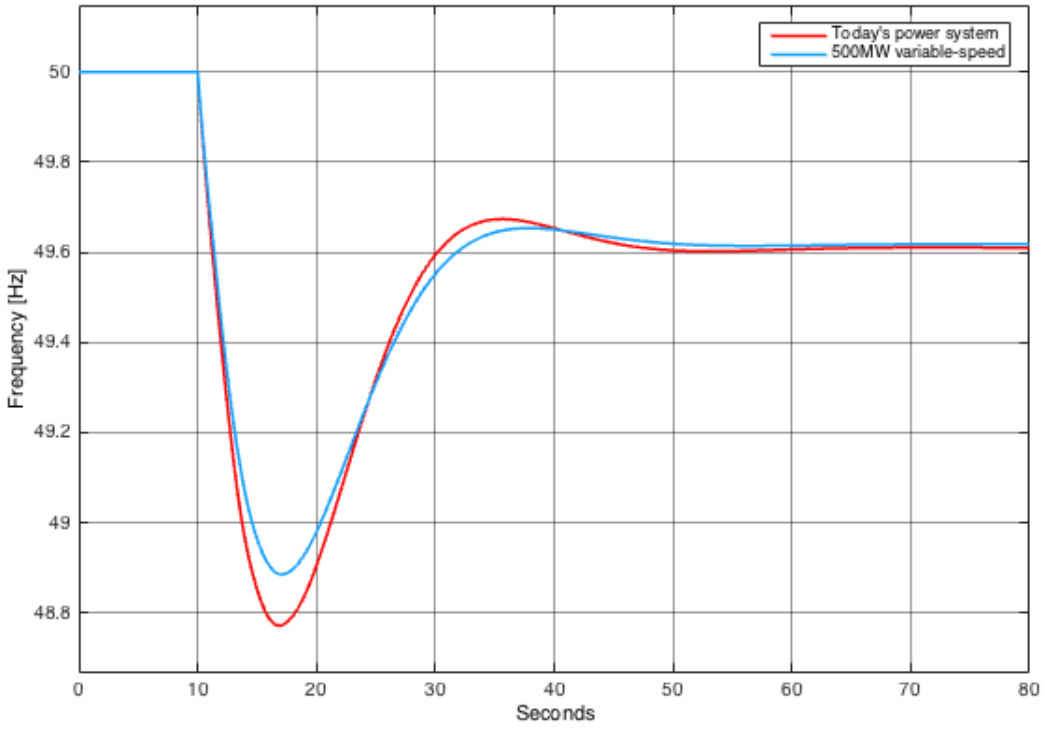

Figure 5.14: Frequency response after 1450 MW load step in SE3.

The location of the fault does not affect the system frequency significantly. Only the magnitude of the fault is found to be of relevance. The fault location will affect the contribution of electrical power for each generator, but the system frequency remains fairly constant for different fault locations. If, however, the spinning reserve in the faulted area is limited, the frequency would suffer, but in this model an upper production limit on the modeled generators is not included. The two simulations show a significant drop in system frequency, to about 48.8 Hz for both of them, see Figure 5.13 and Figure 5.14. As the system under study does not include the entire Nordic grid, the magnitude of the frequency drop caused by the faults will not be equal to the drop for the same scenario in reality. Even so, the model is a reasonable approximation and illustrates that such faults will lead to a drastic drop in system frequency. The simulations also show how only 500 MW of variable-speed hydro improves the frequency response. The results are given in Table 5.4. The percentage of variable-speed hydro capacity in the system is only $\frac{500MW}{29624MW} = 1.69\%$, but the benefits are clearly shown. The frequency nadir of the variable-speed system is only 90.76 % of the normal system's. Another way of quantifying the performance is given in equation 5.1, where $f_{nadir,var}$ and $f_{nadir,nor}$ are the frequency nadirs of the variable-

Table 5.4: Frequency nadir after being subjected to large disturbances.

Disturbance	Frequency nadir normal system [Hz]	Frequency nadir variable-speed system [Hz]
HVDC	48.8141	48.9237
Oskarshamn	48.7716	48.8851

speed hydro system and the normal hydro system respectively.

$$Improvement[\%] = \frac{(50 - f_{nadir,nor}) - (50 - f_{nardir,var})}{50 - f_{nadir,nor}} * 100 \tag{5.1}$$

In both scenarios the improvement by introducing variable-speed hydro is 9.24 %.

5.3.2 Scenario for 2040

The share of the renewable energy sources solar and wind are assumed to increase in the years to come. The Norwegian TSO, Statnett, predicts that almost 50 % of the power production in the Nordic grid in 2040 will come from these sources [2]. Solar- and wind power are non-synchronous generation and will not be directly connected to the grid frequency. To simulate these conditions, solar and wind are indirectly modeled as negative loads, which leads to a decrease in number of hydro plants online. The capacities of the hydropower plants are decreased by 50 % for the futuristic scenario. Another assumption is that the level of consumption is the same. Statnett predicts that the consumption will increase by 25 % by 2040 [2], but for an easier comparison with today's situation, it will be constant.

Table 5.5: Production data and capacity base values for a future Nordic power system.

Area	Production [MW]	Normal hydro capacity [MVA]	Variable-speeed hydro capacity [MVA]
NO1	2249	1406	0
NO2	2707	1192	500
NO3	1680	1050	0
NO4	2504	1565	0
NO5	2597	1623	0
SE1	1353	846	0
SE2	2883	1802	0
SE3	7726	4829	0

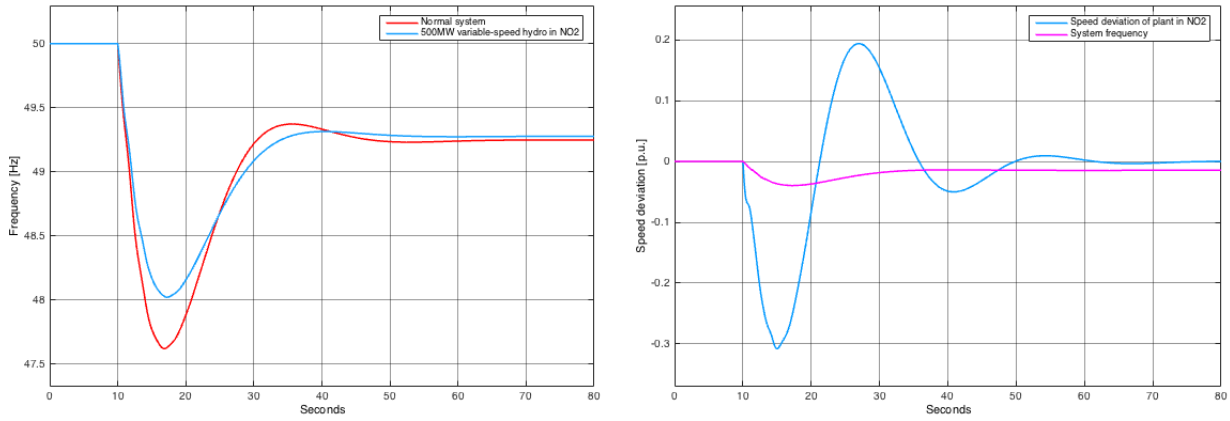

(a) Frequency response (b) Speed deviation

Figure 5.15: Response and after 1400 MW load step in NO2.

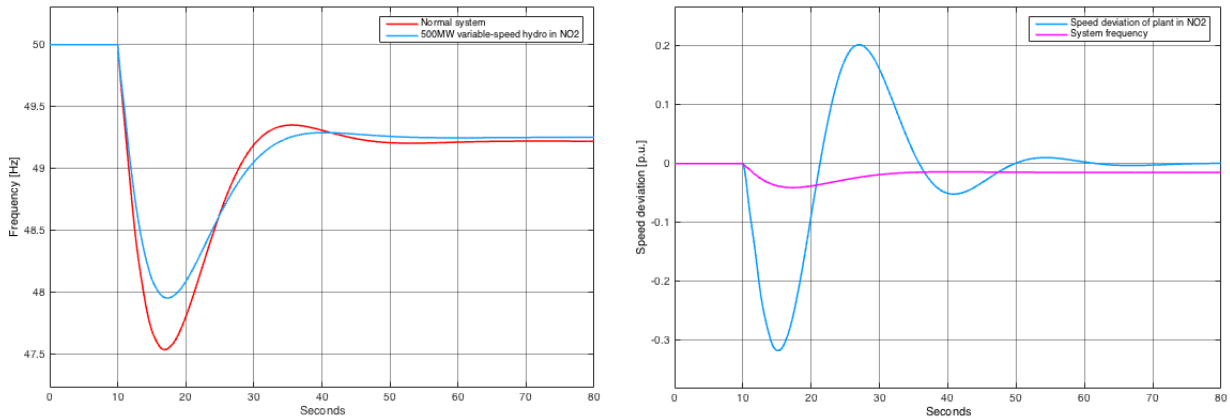

(a) Frequency response (b) Speed deviation

Figure 5.16: Response after 1450 MW load step in SE3.

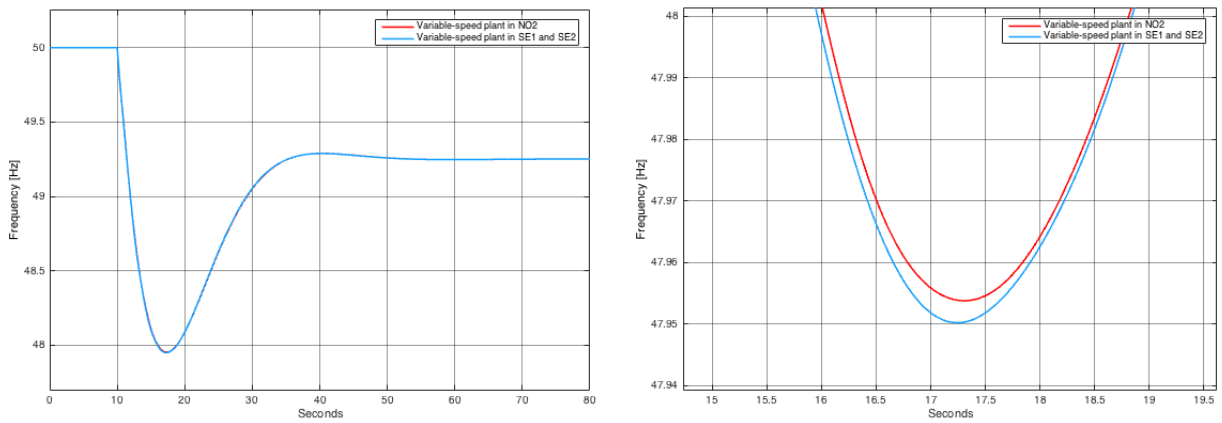

(a) The whole response

(b) Zoomed in at the frequency nadir

Figure 5.17: Frequency response of two systems, each with 500 MW variable-speed hydro.

The system data for the comparison with today's situation is given in Table 5.5. The production levels are the same in each area, but the hydro capacity is reduced by 50 %. The same two grid situations are under study; one with only normal hydro plants and one with 500 MW variable-speed hydro in NO2. For the case with only normal plants, the capacity in NO2 is 1692 MW. The same disturbances are simulated, and the results are shown in Figure 5.15 and Figure 5.16. Figure 5.15 b) and Figure 5.16 b) shows how far from nominal speed the variable-speed plant moves during the disturbance. The speed deviation is dependent on the size of the disturbance. As can be observed, the frequency drop is drastic in both cases. The frequency falls to almost 47.5 Hz, where power plants could start disconnecting to protect themselves and thus create a black-out [1]. The benefit of the variable-speed hydro plant is higher in this case, due to the fact that the share of variable-speed hydro in the system is greater.

It is clear that the capacity of variable-speed hydro has an effect on the frequency stability, and that the location of the fault is of small significance. Therefore only the largest fault, an outage in Oskarshamn, was used for further simulations. A case was made to analyze whether the locations of the variable-speed hydro plants are relevant. The same case as before, with 500 MW VSH in NO2, is compared to a case with 250 MW VSH each in SE1 and SE2. The frequency response, as shown in Figure 5.17, is similar for both cases. The locations of the variable-speed plants are therefore not of great importance.

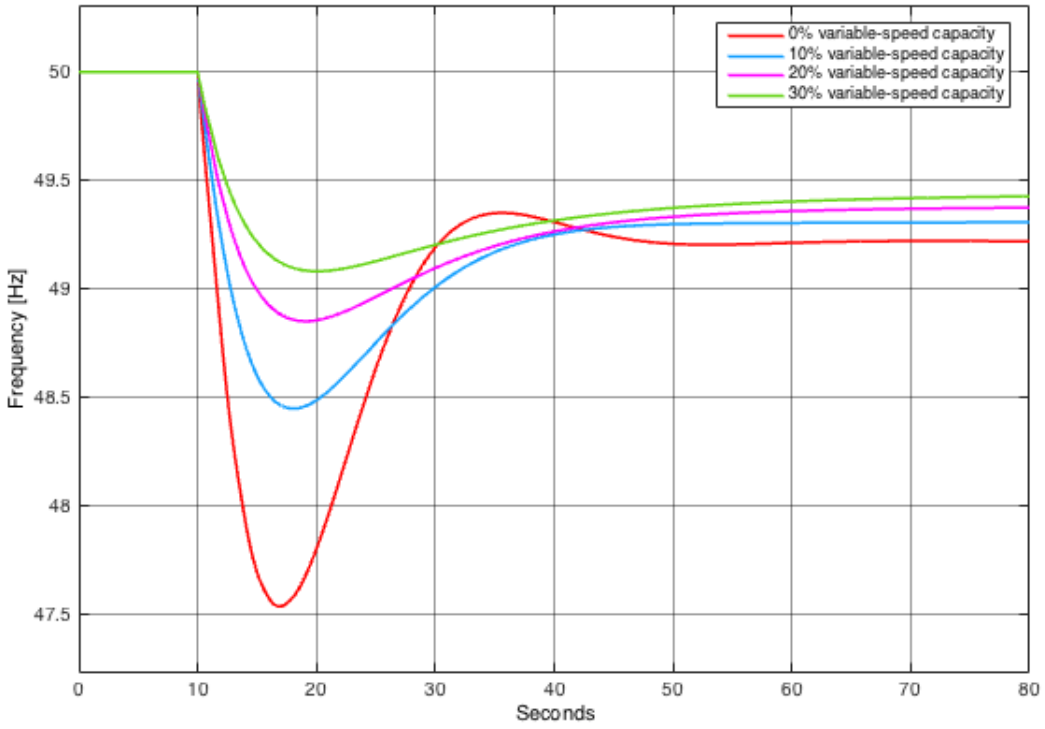

Figure 5.18: Frequency response of systems with different shares of variable-speed hydro capacity after a large disturbance.

To quantify the benefit of variable-speed hydro in the future power system, simulations with different shares of variable-speed hydro capacity are performed. Since the location is not highly significant, the capacity is shared equally between every area except SE3. The production data and the total hydro capacity are still the same as in Table 5.5. The frequency response is given in Figure 5.18, the improvement as calculated from equation 5.1 is shown in Figure 5.19 and the system frequency nadirs, as compared to the reference with only normal plants, are shown in Figure 5.20. As all the mentioned figures illustrate, the benefits are great but decline with increasing capacity of variable-speed hydro. For example the frequency nadir increased by 0.91 Hz by introducing 10 % VSH. Adding another 10 % increased the nadir further by 0.4 Hz. With 30 % VSH the frequency only drops to 49.08 Hz, which is an improvement of over 60 % from the drastic drop of the case with only normal hydro capacity.

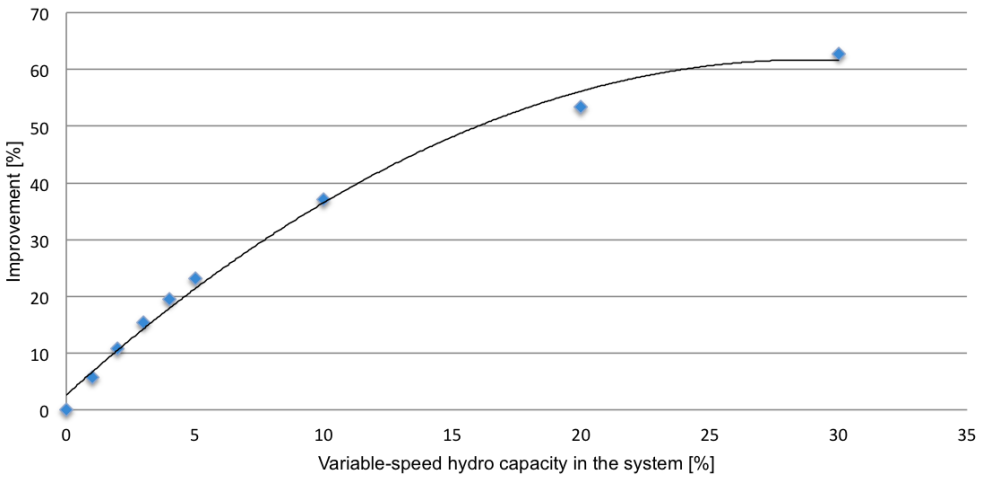

Figure 5.19: The improvement of introducing variable-speed hydro calculated from equation 5.1.

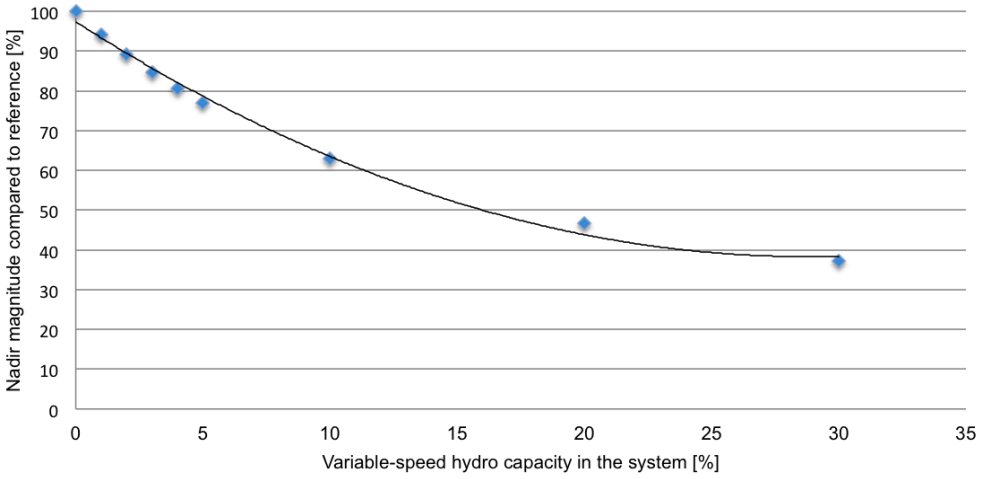

Figure 5.20: The frequency nadirs of variable-speed hydro systems compared to the frequency nadir of a normal system.

Chapter 6

Conclusions and Future Work

6.1 Summary and Conclusions

In this thesis, a model was developed in order to study the power system impacts, with focus on frequency stability, of variable-speed hydro. The model was based on a combination of a hydropower plant model, the swing equation and DC power flow. The software of choice was MATLAB® and Simulink®. Simplifications were made due to the time limitation, and to obtain a fast model. The model uses DC power flow and linearization around an initial operating point, to avoid initialization and the time consuming computations required by an AC model. A voltage source converter is added to the hydropower plant to enable variable-speed operation. The VSC was modeled as the inner current control loop and tuned after the vector control principle. As the model does not contain currents and voltages, the electric frequency is not defined. The scaled mean value of the sum of the generator speeds is used to define a system frequency.

The model was tested against an AC model, developed in [21], to assure that valid simplifications were made. A four bus system, with one variable-speed plant, was used as a basic test case for the validation. The performance was as expected and did not deviate significantly from the AC model. Further, the model was scaled up to approximate parts of the Nordic power system. Before the selected case studies were performed, the characteristics of the model were compared to the frequency response theory. The three stages relevant to this thesis were evident in the model response. The generators closest to the fault experienced rotor swings, while

also having a frequency drop slightly before generators farther from the fault. The frequency nadir was dependent on the governor action and the size of the machines present in the system. Droop control drove the frequency restoration, and the post-fault steady state frequency had an offset from nominal frequency due to the droop settings. Even though the model is a simplification of a real power system, it coincides with theory and can be used to perform fast and reliable frequency studies.

A control scheme was developed with the intention of minimizing the frequency drop, while also restoring the frequency to the post-fault steady state level. As this level is set by droop control, the same principle was applied to the control algorithm of the VSC. The controller acts on frequency deviation, and will produce a power output as a formula dependent on the droop setting. The droop was set equal for every synchronous machine in the system, 12 %. Limiting the frequency drop was done by introducing a derivative term and an integral term in parallel, with the frequency deviation as an input variable. The control scheme proved effective in limiting the frequency drop, due to its ability to utilize the kinetic energy and inject more active power when the frequency was declining.

The model was used to simulate large faults, such as HVDC outage or the outage of the largest unit at Oskarshamn. Such large disturbances could cause the frequency of today's power system to drop beneath 49 Hz during a summer day, when there are less rotating masses connected to the grid. Small amounts of variable-speed hydro brought benefits by increasing the point of the frequency nadir. Only 500 MW, or 1.69 %, gave an improvement of 9.24 % to the frequency drop of today's power system.

As the power system is rapidly changing with the increase in renewable generation, variable-speed hydro could become more relevant. A part of this thesis was to study the possible frequency stability benefits of VSH in the future power system. A possible future power system scenario was simulated by reducing the online hydro capacity by 50 %. The results showed that the frequency drop was drastic for a dimensioning fault. An outage of 1450 MW in Oskarshamn led to a frequency nadir of 47.54 Hz, which is dangerously low and could potentially lead to a

system black-out. Several variable-speed hydro solutions were tested to analyze their impact on frequency stability.

The location of the fault was found to be of little importance to the system frequency. Only the size of the fault was significant to the resulting frequency nadir. The same was found to be true for the location of variable-speed hydro plants. Only the relative share of variable-speed hydro capacity in the total power system was of importance. The improvement, due to increasing shares of VSH capacity, is high for small capacity shares, but has a relative decreasing trend. 10 % VSH capacity gave an improvement of as much as 37 %, while 20 % capacity gave an improvement of 53.4 %. Both results are an improvement from the reference case with only normal hydro plants. The relative decrease is even more evident with further addition of VSH capacity, as 30 % capacity gave an improvement of 62.7 %.

Limiting the frequency drop is seen as the main benefit of VSH during disturbances, since the post-fault steady state frequency is reached at approximately the same time regardless of whether VSH is present in the power system. Variable-speed hydro is able to increase the frequency nadir efficiently, and bring a higher level of frequency stability to the power system. The improvement is made possible by the voltage source converter's ability to act close to instantaneously, and the control mechanism which can make the plant inject more active power during under-frequency events. Due to the variable-speed plant's ability to take more advantage of the kinetic energy stored in the rotor, VSH works well as frequency containment reserve. The results clearly show an improvement in the way the frequency is contained during a large disturbance. The requirements state that the FCR-D should be able to prevent the frequency from dropping below 49.5 Hz following a dimensioning fault. This is not possible with a higher share of non-synchronous renewable energy sources. Even today's grid was not able to prevent such a drop. However, this could be a result of the simplifications made, and the real Nordic grid could have a better performance. The power system of 2040 will not be able to handle such a fault, with the construction it has today and the expected increase in renewable production. A larger share of solar and wind power will decrease the number of hydro plants online and also the amount of spinning reserve available. Lack of spinning reserve decreases the power system's ability to handle large

disturbances. This is confirmed by the comparison between today's- and the future power system. The future power system modeled in this thesis is composed of a smaller number of hydro plants, and therefore has less spinning reserve. The result was a larger drop in frequency following a large disturbance. As demonstrated, variable-speed hydro could be a part of the solution to the frequency stability problem by providing FCR services.

6.2 Discussion

The case studies have given promising results and shown that the benefits of variable-speed hydro are potentially large. However, there are some aspects of the results that can be questioned, and the model comes with limitations due to assumptions and simplifications made.

Many of the simplifications were tested in section 5.1, where the model was compared to an AC model in a test grid situation. The plant's electromechanical dynamics have only two state variables, while the AC model uses a fifth-order model. The differences between the two models were minimal, but there are uncertainties as to whether the size of the network could have an impact. The test case network was a four bus system with only four generators. The Nordic grid is composed of a large number of generators, and the simplification made to each generator could potentially add up to a large deviation.

The most unexpected behaviour of the model was the change in electrical power produced by the generators. For the small test case network, the parameter experienced large and high-frequent oscillations. The oscillations come from large variations in the rotor angle of the generators and the difference between them. An interconnected network, such as the Nordic grid, was found to have a less oscillating- and more expected behaviour. An interconnected grid will provide natural damping which leads to less variation between the rotor angles and a more realistic response of the electrical power output. Another uncertainty regarding this variable is the behaviour of the accumulated generation in SE3. The mix of hydropower and nuclear power is modeled as a hydropower plant with a droop setting of 50 %. The droop led to a realistic post-fault steady state contribution, but the contribution during the frequency drop is unrealistic,

because nuclear power does not contribute to primary frequency control in Norway and Sweden. The large inertia and capacity of the area's modeled plant contributed in containing the frequency drop. The area's large contribution will, however, improve the frequency response and increase the frequency nadir compared to a more accurate model of the area, where nuclear power is not able to work as primary frequency control. Since the accumulated generation of SE3 gives the same response for all case studies, it will not affect the study of the benefits of variable-speed hydro. Due to the fact that a more realistic model would lower the frequency nadir, the need for variable-speed hydro would actually be greater.

Further, the response time of the voltage source converter should be around 10 times slower, due to the absence of DC voltage control. This could affect the performance of the VSH plants, but the response is still much faster than the slow electromechanics that determine the frequency. From theory, the frequency after a disturbance is dependent on the amount of available spinning reserve in the system. The spinning reserve and the droop control are parameters that introduce uncertainties to the results. The total capacity online is calculated from the production data at a specific instant in time, while the droop setting is the same for all generators. Hence, each area contributes with a spinning reserve relative to its capacity and does not have an upper limit. The distribution of spinning reserve is also well spread over the entire network, which is not always the case. Such an even distribution of spinning reserve leads to greater frequency stability. Again, the simplifications made are equal for all cases and therefore do not diminish the results of the study of the benefits of variable-speed hydro. The greatest uncertainty is how much lower the frequency would drop in reality, not how much VSH would improve the relative performance. The advantage of the model is that the parameters, such as the droop and the capacity of each area, can easily be changed to simulate a different scenario.

Even though the model is flexible, it has its limitations. First of all, it is only able to analyze frequency stability. Other forms of power system stability, such as rotor angle- and voltage stability, are ignored. Variable-speed hydro could potentially be beneficial to the voltage stability as well, due to the converter's ability to also control reactive power. This potential benefit is not possible to study with the developed model, because all voltages are assumed constant. The

model is also only equipped to simulate under-frequency events. The reported main benefit of variable-speed hydro is the ability to control power in pump mode. To enable pump mode for the variable-speed plant, a back-to-back VSC is necessary. Only a simplified version of a VSC is present in the model, and the frequency response in pump mode would not be representative of a real variable-speed plant. The plant itself is modeled as a negative load, which limits the amount of variable-speed hydro capacity in the system. As the frequency is a function of the speed of the generators of normal hydro plants, there must be a certain amount of normal hydro capacity in each area. With close to zero normal hydro plants present, the system frequency would become unstable.

Further limitations are that the operation of the variable-speed plants is disregarded. The model assumes that every VSH plant is in generation mode and at nominal speed at the time of the disturbance. It is fully possible that such a plant is in pump mode, and therefore cannot contribute in the same way. The physical limitations of operating away from the nominal point are not taken into account. Phenomena such as cavitation and vibration are not in the scope of this thesis, and are therefore ignored. The market perspective is also outside the scope, so how the plant will work in the reserve markets is not examined.

6.3 Recommendations for Future Work

Variable-speed hydro has shown interesting capabilities, especially the ability to improve the frequency stability in the future Nordic grid. This benefit, along with the ability to control power in pump mode, makes VSH a subject that should be further researched. By widening the scope, and looking deeper into the dynamics of the plant as well as the effect it has on the power system, more characteristics could be identified. This section provides suggestions for future work on the topic.

A more thorough examination of the effects of variable-speed hydro on the power system is preferable before making it a reality. This thesis has quantified potential benefits, but in a simplified grid with several important elements ignored. Before VSH can be approved as FCR, one

must be sure that it does not create further problems for the grid, as this is a requirement for such reserves. To be able to analyze every aspect of the change VSH brings to the power system, a more complicated model should be utilized. The accuracy of the model could be improved if several of the components of the model are expanded, such as the hydropower plant model, the VSC and the grid itself. For example should the model include a more detailed representation of each bidding area, and be able to take into account that nuclear power does not take part in primary frequency control. The aggregated Nordic model in PSS®E, Nordic44, could be appropriate for further research. In this way, more varieties of analysis can be made, such as voltage stability analysis. VSH's ability to improve voltage stability was outside the scope of this thesis, but is an interesting subject that needs further work. The plant's contribution to both frequency- and voltage stability requires a control strategy. The control strategy developed in this thesis was simple and had one goal; limiting the frequency drop after a disturbance. A more advanced control algorithm could prevent the rotor from returning to nominal speed during the frequency restoration stage. A possible strategy is closing the inlet gate right before the frequency nadir. This cannot be done by a simple PI-, PD- or PID controller reacting to the deviation from nominal frequency. Selection of controller, control variable and control strategy for the purpose of dampening the frequency restoration is an interesting research topic. Another control aspect is the market strategy. A VSH plant including pump mode should develop a strategy that can bring additional revenues for the plant owner.

This thesis focused on modeling a converter-fed synchronous machine. Utilizing a doubly-fed induction machine is another way of realizing variable-speed to a plant, and is the most used technology today. Research comparing the two, with respect to frequency stability for the grid, will be interesting for future decision makers. Finally, comparison of the models to a real variable-speed plant should be conducted for validation. Few plants are in operation today, but Switzerland has several projects that could be of research interest.

Bibliography

[1] J. Machowski, J. Bialek, and J. R. Bumby, *Power system dynamics and stability*. John Wiley & Sons, 2nd ed., 2008.

[2] Statnett, "Langsiktig markedsanalyse - Norden og Europa 2016-2040," 2016.

[3] ENTSO-E, "System operation agreement," 2014.

[4] M. Valavi and A. Nysveen, "Variable-speed operation of hydropower plants: Past, present, and future," in *Electrical Machines (ICEM), 2016 XXII International Conference on*, pp. 640–646, IEEE, 2016.

[5] H. Schlunegger and A. Thöni, "100 mw full-size converter in the grimsel 2 pumped-storage plant," in *Proc. 2013 HYDRO Conference*, 2013.

[6] Linth-Limmern, "Linthal - securing future electricity supply." https://www.gerenewableenergy.com/stories/linthal-securing-future. Accessed: 2018-05-11.

[7] Nant-De-Drance, "Une nouvelle centrale de pompage-turbinage." http://www.nant-de-drance.ch/projet/generalites/. Accessed: 2018-05-11.

[8] P. Kundur, J. Paserba, V. Ajjarapu, G. Andersson, A. Bose, C. Canizares, N. Hatziargyriou, D. Hill, A. Stankovic, C. Taylor, *et al.*, "Definition and classification of power system stability ieee/cigre joint task force on stability terms and definitions," *IEEE transactions on Power Systems*, vol. 19, no. 3, pp. 1387–1401, 2004.

[9] K. Uhlen, "Power System Stability and Control." Lecture notes for the course TET4180 at Department of Electric Power Engineering, Norwegian University of Science and Technology, 2018.

[10] A. M. Pirbazari, "Ancillary services definitions, markets and practices in the world," in *Transmission and Distribution Conference and Exposition: Latin America (T&D-LA), 2010 IEEE/PES*, pp. 32–36, IEEE, 2010.

[11] Statnett, "Primærreserver (FCR)." http://www.statnett.no/Drift-og-marked/Markedsinformasjon/Primarreserver/. Accessed: 2018-03-06.

[12] Statnett, "Systemdrifts- og markedsutviklingsplan 2014-20. tiltaksplan for sikker og effektiv drift av kraftsystemet," 2014.

[13] Statnett, "Vilkår for tilbud, aksept, rapportering og avregning i marked for FCR," 2016.

[14] B. Stott, J. Jardim, and O. Alsaç, "Dc power flow revisited," *IEEE Transactions on Power Systems*, vol. 24, no. 3, pp. 1290–1300, 2009.

[15] K. Uhlen, "DC Power Flow and DC-OPF." Lecture notes for the course TET4115 at Department of Electric Power Engineering, Norwegian University of Science and Technology, 2015.

[16] S. Hadi, *Power System Analysis*. McGraw-Hill, 2nd ed., 2002.

[17] V. V. Vadlamudi, "Refresher on the Fundamentals of Power Systems." Lecture notes for the course TET4115 at Department of Electric Power Engineering, Norwegian University of Science and Technology, 2015.

[18] MathWorks, "What is MATLAB." https://se.mathworks.com/discovery/what-is-matlab.html. Accessed: 2018-04-17.

[19] MathWorks, "Simulink." https://se.mathworks.com/products/simulink.html. Accessed: 2018-04-17.

[20] K. G. Andersen, "Area Based Secondary Frequency Control in the Nordic Power System," Master's thesis, Norwegian University of Science and Technology, 2016.

[21] A. S. Øverjordet, "Synthetic Inertia from Wind Farms," Master's thesis, Norwegian University of Science and Technology, 2014.

[22] E. Aronsveen, "A Review of the Concept and Possibilities of Variable-Speed Hydro." Project work, Norwegian University of Science and Technology, December 2017.

[23] F. Demello, R. Koessler, J. Agee, P. Anderson, J. Doudna, J. Fish, P. Hamm, P. Kundur, D. Lee, G. Rogers, *et al.*, "Hydraulic-turbine and turbine control-models for system dynamic studies," *IEEE Transactions on Power Systems*, vol. 7, no. 1, pp. 167–179, 1992.

[24] S. Jakobsen, K. Uhlen, and X. Bombois, "Identification of hydro turbine governors using PMU data," 2017.

[25] ENTSO-E, "Maximum Net Transfer Capacities." https://www.nordpoolgroup.com/globalassets/download-center/tso/max-ntc.pdf. Accessed: 2018-02-12.

[26] Nord Pool AS, "Production data." https://www.nordpoolgroup.com/Market-data1/Power-system-data/Production1/Production1/ALL1/Hourly1/?view=chart. Accessed: 2018-05-01.

Appendix A

Acronyms

AC Alternating current

AGC Automatic generation control

AVR Automatic voltage regulator

CFSM Converter-fed synchronous machine

DC Direct current

DFIM Doubly-fed induction machine

FCR Frequency containment reserve

HVDC High voltage direct current

IGBT Insulated-gate bipolar transistor

MMC Modular multilevel converter

PI Proportional integral

PLL Phase locked loop

p.u. Per unit

PV Photovoltaic

PWM Pulse width modulation

TSO Transmission system operator

VSC Voltage source converter

VSH Variable-speed hydro

Appendix B

Block Diagrams and System Parameter Values

B.1 Block Diagrams

B.1.1 Top Level

The top level of the model comprises eight areas, each with one generator and a load. Two function blocks are present to calculate the system frequency and the change in electrical power. The variable-speed plant is a negative load. In this example, only NO2 has a variable-speed hydro capacity.

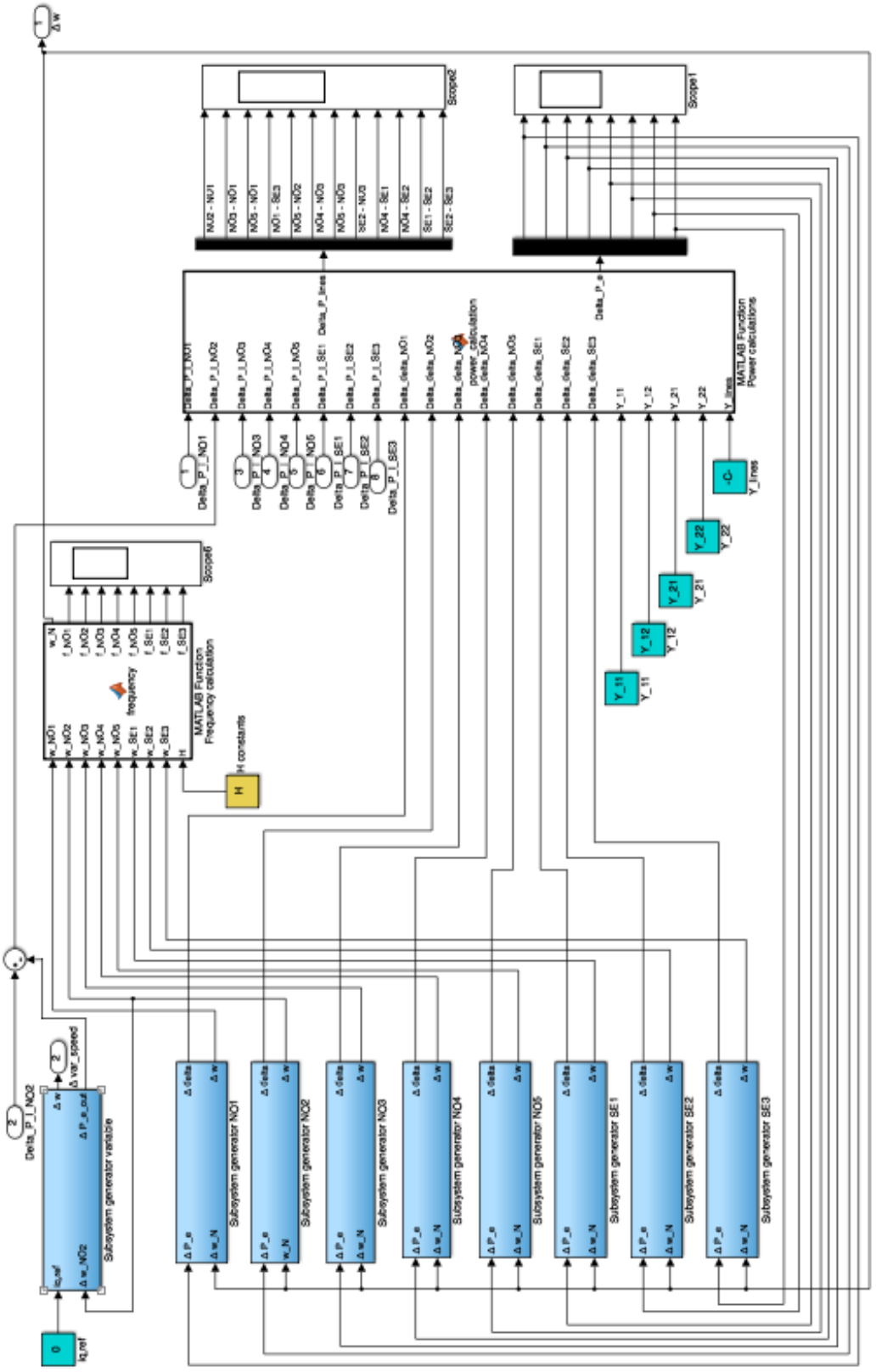

Figure B.1: Main level of the Nordic power system model, with load step blocks as input and the system frequency as the output variable. In this example, only area NO2 contains variable-speed capacity.

B.1.2 Normal Hydro Plant

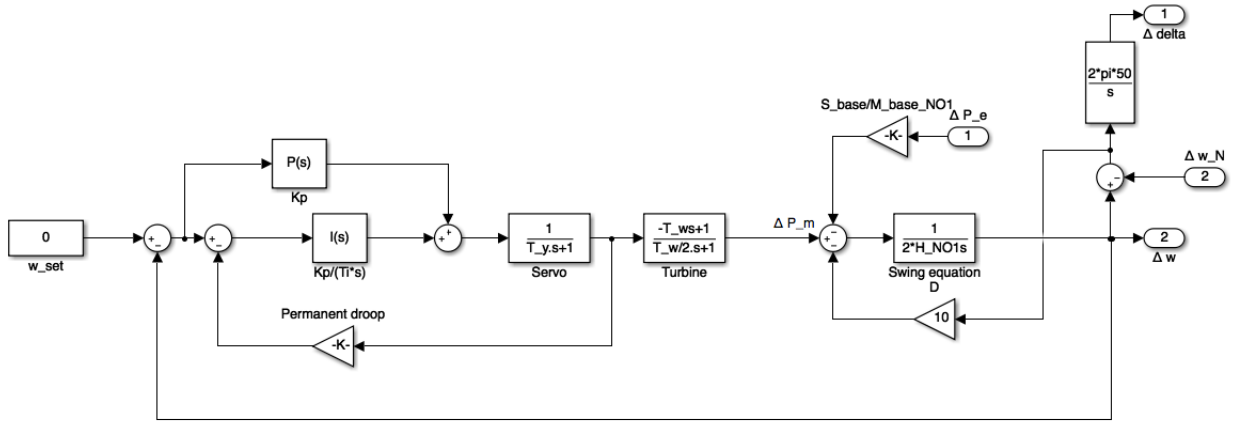

Figure B.2: Block diagram of a normal hydro plant.

B.1.3 Variable-Speed Hydro Plant

The variable-speed plant is slightly different, with no need for a damping term, and the fact that the electric power reference, ΔP_e, is an input variable from the VSC.

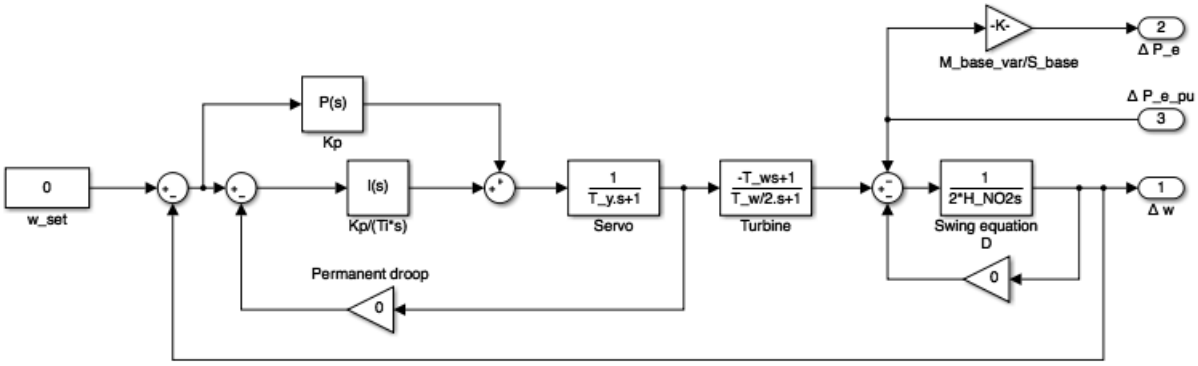

Figure B.3: Block diagram of a variable-speed hydro plant, with the electrical power as an input variable from the VSC.

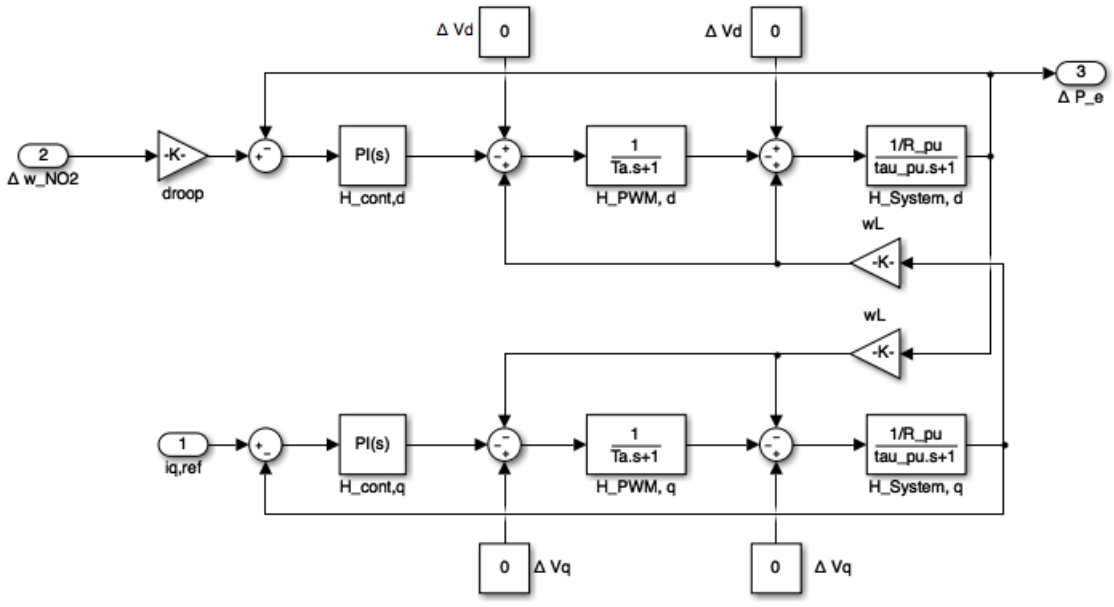

Figure B.4: Block diagram of the VSC. The input variable is the frequency deviation from nominal frequency, and the output variable is change in electrical power.

B.2 Parameter Values

Table B.1: Parameters values for the Nordic power system model. The parameter values were chosen in order to get a suitable model for the purpose of this thesis.

Parameter	Value	Unit
x'_{d1}	0.6	p.u.
x'_{d2}	0.7	p.u.
x'_{d3}	0.9	p.u.
x'_{d4}	0.7	p.u.
x'_{d5}	0.6	p.u.
x'_{d6}	0.8	p.u.
x'_{d7}	0.7	p.u.
x'_{d8}	0.8	p.u.
H_{NO1}	3,494	s
H_{NO2}	3,370	s
H_{NO3}	3,558	s
H_{NO4}	3,592	s
H_{NO5}	3,5	s
H_{SE1}	4,602	s
H_{SE2}	3,3	s
H_{SE3}	5,403	s
$\rho_{NO1...SE2}$	0,12	-
ρ_{SE3}	0,50	-
$D_{NO1...SE3}$	10	p.u.

Table B.2: Line reactances and maximum transfer capabilities for the Nordic power system model.

Line reactance	Value [p.u.]	Maximum transfer capability [MVA]
$x_{11,12}$	$\frac{1}{3,5}$	3500
$x_{11,13}$	$\frac{1}{0,5}$	500
$x_{11,15}$	$\frac{1}{3,9}$	3900
$x_{11,18}$	$\frac{1}{2,145}$	2145
$x_{12,15}$	$\frac{1}{0,6}$	600
$x_{13,14}$	$\frac{1}{1,2}$	1200
$x_{13,15}$	$\frac{1}{0,5}$	500
$x_{13,17}$	$\frac{1}{1}$	1000
$x_{14,16}$	$\frac{1}{0,7}$	700
$x_{14,17}$	$\frac{1}{0,3}$	300
$x_{16,17}$	$\frac{1}{3,3}$	3300
$x_{17,18}$	$\frac{1}{7,3}$	7300

Appendix C

Admittance Matrix

The four sub-matrices from equation 3.1 are expressed as:

$$Y_{11} = \begin{bmatrix} \frac{1}{x_{d1}} & 0 & 0 & 0 & 0 & 0 & 0 & 0 \\ 0 & \frac{1}{x_{d2}} & 0 & 0 & 0 & 0 & 0 & 0 \\ 0 & 0 & \frac{1}{x_{d3}} & 0 & 0 & 0 & 0 & 0 \\ 0 & 0 & 0 & \frac{1}{x_{d4}} & 0 & 0 & 0 & 0 \\ 0 & 0 & 0 & 0 & \frac{1}{x_{d5}} & 0 & 0 & 0 \\ 0 & 0 & 0 & 0 & 0 & \frac{1}{x_{d6}} & 0 & 0 \\ 0 & 0 & 0 & 0 & 0 & 0 & \frac{1}{x_{d7}} & 0 \\ 0 & 0 & 0 & 0 & 0 & 0 & 0 & \frac{1}{x_{d8}} \end{bmatrix} \tag{C.1}$$

$$Y_{12} = \begin{bmatrix} -\frac{1}{x_{d1}} & 0 & 0 & 0 & 0 & 0 & 0 & 0 \\ 0 & -\frac{1}{x_{d2}} & 0 & 0 & 0 & 0 & 0 & 0 \\ 0 & 0 & -\frac{1}{x_{d3}} & 0 & 0 & 0 & 0 & 0 \\ 0 & 0 & 0 & -\frac{1}{x_{d4}} & 0 & 0 & 0 & 0 \\ 0 & 0 & 0 & 0 & -\frac{1}{x_{d5}} & 0 & 0 & 0 \\ 0 & 0 & 0 & 0 & 0 & -\frac{1}{x_{d6}} & 0 & 0 \\ 0 & 0 & 0 & 0 & 0 & 0 & -\frac{1}{x_{d7}} & 0 \\ 0 & 0 & 0 & 0 & 0 & 0 & 0 & -\frac{1}{x_{d8}} \end{bmatrix} \tag{C.2}$$

$$Y_{21} = \begin{bmatrix} -\frac{1}{x_{d1}} & 0 & 0 & 0 & 0 & 0 & 0 & 0 \\ 0 & -\frac{1}{x_{d2}} & 0 & 0 & 0 & 0 & 0 & 0 \\ 0 & 0 & -\frac{1}{x_{d3}} & 0 & 0 & 0 & 0 & 0 \\ 0 & 0 & 0 & -\frac{1}{x_{d4}} & 0 & 0 & 0 & 0 \\ 0 & 0 & 0 & 0 & -\frac{1}{x_{d5}} & 0 & 0 & 0 \\ 0 & 0 & 0 & 0 & 0 & -\frac{1}{x_{d6}} & 0 & 0 \\ 0 & 0 & 0 & 0 & 0 & 0 & -\frac{1}{x_{d7}} & 0 \\ 0 & 0 & 0 & 0 & 0 & 0 & 0 & -\frac{1}{x_{d8}} \end{bmatrix} \tag{C.3}$$

$$Y_{22} = \begin{bmatrix} y_{11} & -\frac{1}{x_{11,12}} & -\frac{1}{x_{11,13}} & 0 & -\frac{1}{x_{11,15}} & 0 & 0 & -\frac{1}{x_{11,18}} \\ -\frac{1}{x_{11,12}} & y_{22} & 0 & 0 & -\frac{1}{x_{12,15}} & 0 & 0 & 0 \\ -\frac{1}{x_{11,13}} & 0 & y_{33} & -\frac{1}{x_{13,14}} & -\frac{1}{x_{13,15}} & 0 & -\frac{1}{x_{13,17}} & 0 \\ 0 & 0 & -\frac{1}{x_{13,14}} & y_{44} & 0 & -\frac{1}{x_{14,16}} & -\frac{1}{x_{14,17}} & 0 \\ -\frac{1}{x_{11,15}} & -\frac{1}{x_{12,15}} & -\frac{1}{x_{13,15}} & 0 & y_{55} & 0 & 0 & 0 \\ 0 & 0 & 0 & -\frac{1}{x_{14,16}} & 0 & y_{66} & -\frac{1}{x_{16,17}} & 0 \\ 0 & 0 & -\frac{1}{x_{13,17}} & -\frac{1}{x_{14,17}} & 0 & -\frac{1}{x_{16,17}} & y_{77} & -\frac{1}{x_{17,18}} \\ -\frac{1}{x_{11,18}} & 0 & 0 & 0 & 0 & 0 & -\frac{1}{x_{17,18}} & y_{88} \end{bmatrix} \tag{C.4}$$

The diagonal elements of Y_{22} are given as:

$$\begin{aligned}
y_{11} &= \frac{1}{x_{d1}} + \frac{1}{x_{11,12}} + \frac{1}{x_{11,13}} + \frac{1}{x_{11,15}} + \frac{1}{x_{11,18}} \\
y_{22} &= \frac{1}{x_{d2}} + \frac{1}{x_{11,12}} + \frac{1}{x_{12,15}} \\
y_{33} &= \frac{1}{x_{d3}} + \frac{1}{x_{11,13}} + \frac{1}{x_{13,14}} + \frac{1}{x_{13,15}} + \frac{1}{x_{13,17}} \\
y_{44} &= \frac{1}{x_{d4}} + \frac{1}{x_{13,14}} + \frac{1}{x_{14,16}} + \frac{1}{x_{14,17}} \\
y_{55} &= \frac{1}{x_{d5}} + \frac{1}{x_{11,15}} + \frac{1}{x_{12,15}} + \frac{1}{x_{13,15}} \\
y_{66} &= \frac{1}{x_{d6}} + \frac{1}{x_{14,16}} + \frac{1}{x_{16,17}} \\
y_{77} &= \frac{1}{x_{d7}} + \frac{1}{x_{13,17}} + \frac{1}{x_{14,17}} + \frac{1}{x_{16,17}} + \frac{1}{x_{17,18}} \\
y_{11} &= \frac{1}{x_{d8}} + \frac{1}{x_{11,18}} + \frac{1}{x_{17,18}}
\end{aligned} \tag{C.5}$$

The line flow matrix of the system is given below. Negative signs are placed in order to get positive flows.

$$Y_{lines} = \begin{bmatrix}
-\frac{1}{x_{11,12}} & \frac{1}{x_{11,12}} & 0 & 0 & 0 & 0 & 0 & 0 \\
-\frac{1}{x_{11,13}} & 0 & \frac{1}{x_{11,13}} & 0 & 0 & 0 & 0 & 0 \\
-\frac{1}{x_{11,15}} & 0 & 0 & 0 & \frac{1}{x_{11,15}} & 0 & 0 & 0 \\
\frac{1}{x_{11,18}} & 0 & 0 & 0 & 0 & 0 & 0 & -\frac{1}{x_{11,18}} \\
0 & -\frac{1}{x_{12,15}} & 0 & 0 & \frac{1}{x_{12,15}} & 0 & 0 & 0 \\
0 & 0 & -\frac{1}{x_{13,14}} & \frac{1}{x_{13,14}} & 0 & 0 & 0 & 0 \\
0 & 0 & -\frac{1}{x_{13,15}} & 0 & \frac{1}{x_{13,15}} & 0 & 0 & 0 \\
0 & 0 & -\frac{1}{x_{13,17}} & 0 & 0 & 0 & \frac{1}{x_{13,17}} & 0 \\
0 & 0 & 0 & \frac{1}{x_{14,16}} & 0 & -\frac{1}{x_{14,16}} & 0 & 0 \\
0 & 0 & 0 & \frac{1}{x_{14,17}} & 0 & 0 & -\frac{1}{x_{14,17}} & 0 \\
0 & 0 & 0 & 0 & 0 & \frac{1}{x_{16,17}} & -\frac{1}{x_{16,17}} & 0 \\
0 & 0 & 0 & 0 & 0 & 0 & \frac{1}{x_{17,18}} & -\frac{1}{x_{17,18}}
\end{bmatrix} \tag{C.6}$$

Appendix D

System Parameters and Tuning of the Voltage Source Converter

Table D.1: System parameters

Parameter	Value
Line resistance, R	0.01 p.u.
Line reactance, X_L	0.1 p.u.
DC-link capacitor, C	0.5 p.u.
Voltage constant, K	1
Switching frequency	1 kHz
Measurement delay	2 ms

Table D.2: Control parameters for inner current control

Parameter	Value
K_p	0.0637
T_i	0.0318
τ_a	2.5 ms